공학박사학위논문

Complex flow behaviors of concentrated alumina suspensions in pressure-driven flow

압력 구배 흐름에서의 고농도 알루미나 현탁액의 복잡 거동

2013년 8월

서울대학교 대학원

화학생물공학부

한 우 주

Abstract

Complex flow behaviors of concentrated alumina suspensions in pressure-driven flow

Woojoo Han

School of Chemical and Biological Engineering

The Graduate School

Seoul National University

A new approach was taken to understand the flow behavior of concentrated particle suspensions in pressure-driven capillary flow. The flow of concentrated alumina suspensions in a slit channel was visualized depending on dispersion states, coagulated system and well-dispersed system, with modified capillary rheometer. The complex flow behaviors of suspensions including the flow development in solid-liquid transition process were quantitatively described in terms of flow profile and pressure fluctuation.

The suspensions showed complex flow behaviors; unique solid-liquid transition and shear banding. In the solid-liquid transition, there was no-flow at first and continuous change of flow profile was observed with time. At low shear rates in particular, the suspensions exhibited shear banded flow profile which could be divided into 3 regions: the region with low flow rate near the

wall, the region with rapid increase of flow velocity to maximum, and the region of velocity plateau. The banding in pressure-driven flow was different from that in Couette flow. The banding of concentrated alumina suspensions was unique in that sluggish velocity profile was pronounced and two inflection points in velocity profile was exhibited. Based on both flow visualization and measurement of shear stress, it was found that the shear banded flow profile in pressure driven slit channel flow was strongly correlated with shear stress.

For the coagulated alumina suspension, the shear stress showed an N-curve that included a region of stress decrease with an increase in shear rate followed by a monotonic increase. Depending on the region in the stress curve, the flow profile changed from a shear banded profile with no-flow or sluggish flow rate closed to the channel wall and plug flow at channel center to a plug-like flow profile similar to the Newtonian fluid. In addition, it was observed that the transient flow behavior over time at high shear rate in liquid state experienced all of the steady state flow profiles at lower shear rates in solid-liquid transition. During the solid-liquid transition, the flow profile was found to be shear banded, and the pressure profile did not reach a steady state but fluctuated with a characteristic time period. As the solid concentration increased for the coagulated system, the flow profile in the solid-liquid transition region (stress-decay region) exhibited more complex flow behavior of very large no-flow region along with an asymmetric flow and its fluctuations. With the FT analysis of pressure fluctuation and flow fluctuation, it was determined that pressure fluctuation had the same time

period with the flow profile fluctuation and the flow profile change in the slit channel had close relationship with the pressure change, which is meaning of that the pressure fluctuation is caused by the complex flow behavior inside the channel.

In contrast with coagulated suspension, the well-dispersed suspension with low solid concentration showed only a monotonic increase of shear stress in the range of shear rates we could measure, indicating that the suspension was in liquid state. The flow profile was plug-like, and the pressure was fluctuating without any characteristic time period. However, the well-dispersed suspensions with higher solid concentration exhibited complex flow behaviors similar to coagulated suspension such as unique solid-liquid transition and shear banded flow profile.

In this study, shear banding of concentrated alumina suspensions in slit channel flow was visualized and quantitatively analyzed. We expect this approach can be an effective method to understand the flow behavior of particulate suspensions in the pressure-driven flow which is typical in industrial processing.

Keywords: complex flow, shear banding, pressure-driven flow, concentrated suspensions, solid-liquid transition, pressure fluctuation

Student Number: 2006-21394

Contents

List of figures

Chapter 1. Introduction

1.1 General introduction

Electronic materials used in LED (Light Emitting Diode), LCD (Liquid Crystal Display), MLCC (Multi-Layer Ceramic Capacitor) and energy materials used in solar cell, Li-ion battery as well as commodities such as paint, cosmetic products, cement pastes are complex fluids which consist of organic/inorganic particles, polymers and solvents. Concentrated particulate suspension, which is a kind of complex fluid, often exhibits complex and diverse formation and change of internal structures depending on the flow condition. As the solid concentration increases, the complexity increases and many interesting behaviors such as yielding, shear banding, and shear thickening, which do not occur at low concentration are observed.

Suspensions typically show shear thinning behavior, and shear thickening is observed only at high concentration. Shear thickening happens when the suspension experiences high shear flow and becomes more intensified with high solid concentration. Also, the size and the shape of the particle affect the shear thickening behavior (Lee and Wagner 2003; Maranzano and Wagner 2001a 2001b). The shear thickening behavior can disturb the flow during processing and may form heterogeneous microstructure in local or sometimes in whole dimension of the flow geometry (Lootens et al. 2005). In addition, large shear stress fluctuation was observed above the critical shear rate for shear thickening (Maranzano and Wagner 2001b).

Yielding is a kind of solid-liquid transition. In the case of concentrated

particle suspensions, the fluid does not experience simple yielding such that homogeneous deformation is exhibited up to a critical value of shear stress in the solid regime, but shows more complex and discrete yielding behavior in which non-homogeneous deformation is exhibited at low shear rate regime while homogeneous deformation can be shown at high shear rates (Coussot 2005). Similar to shear thickening, yielding or solid-liquid transition is also affected by concentration, particle size and its distribution, surface potential, and process conditions (Johnson et al. 2000).

Another complex behavior of concentrated suspension is shear banding in which fluid flows with more than two shear-rate layers or two phases in shear flow. Depending on the shape and direction of layers, it could be divided into gradient-banding and vorticity-banding (Dhont and Briels 2008; Fielding 2007; Manneville 2008; Olmsted 2008; Ovarlez et al. 2009). As shear banding is related to the transition from solid to liquid state, it can be thought of as a part of discrete yielding or complex solid-liquid transition which contains non-homogeneous flow field in specific shear rate regime. Viscosity and other properties of concentrated suspensions are functions of shear rate. As shear-banding means that the fluid experiences different flow environments during the flow at the same time, it may cause flow instability which leads to difficulties in process control.

Processing of concentrated suspensions involve various processes such as mixing, transportation, coating, and drying (Kim et al. 2009). In these processes, not only drag flow but also elongational, pressure-driven, contraction or expansion flow may arise. The suspensions form various

internal structures during the flow, resulting in the complex flow behaviors mentioned above. Such complex flow behaviors lead to non-uniform structure development, potentially causing unstable processes with large stress fluctuations. In this sense, it is important to understand and control the complex flow of these fluids to achieve stable process with high productivity and quality.

There were researches on yielding, shear banding, and shear thickening of concentrated suspensions because of the industrial and academic necessity (Mewis and Wagner 2012). To visualize and understand the complex flow behaviors of concentrated suspensions, SANS, MRI, and confocal microscopy were used (Besseling et al. 2009; Besseling et al. 2010; Coussot et al. 2008; Mansard and Colin 2012; Maranzano and Wagner 2001b). However most of the studies were limited to low shear rate flow in rotational rheometer. Only a few were focused on the pressure driven flow that appears in actual processes such as transportation or coating (Isa et al. 2007). Therefore, more systematic study on the pressure driven flow of concentrated suspension is necessary.

The goal of this thesis is to visualize and to characterize *in-situ* flow of concentrated particle suspensions in slit channel flow which is driven by pressure gradient. In this study, a conventional capillary rheometer was modified to *in-situ* visualize flow and to measure the rheological properties including precise pressure profiles. Using this modified capillary rheometer, the flow of concentrated particle suspensions in slit channel was visualized, characterized, and analyzed quantitatively.

In this thesis, the flows of concentrated alumina suspensions of two different dispersion states (coagulated and well-dispersed) in a slit channel over various flow conditions were visualized and analyzed. The dispersion state of the suspension was controlled by adjusting the surface charge of the particles. In addition, the flow behavior was analyzed and compared with shear stress and pressure variation.

1.2 Outline of the Thesis

This thesis is organized as follow. In Chapter 2, the background of this work and previous research relating this work are introduced. This chapter comprises two sections. The first section covers the theory on colloidal interaction effecting on dispersion state of suspension. The second section covers the reviews of previous research about shear banding behavior of concentrated suspensions. Chapter 3 describes materials involved in this work followed by the methods of suspension preparation. Modification of conventional capillary rheometer and data analysis procedure are also outlined in this chapter. In chapter 4, flow visualization results and its analysis with pressure fluctuation and shear stress curve are discussed. This chapter includes three sections. The first section and second section cover the results of well-dispersed alumina suspensions and coagulated alumina suspension, respectively. In last section of this chapter, flow instabilities of coagulated alumina suspension having high solid concentration and its analysis with pressure fluctuation analysis are discussed. The conclusion from the work is drawn in last chapter.

Chapter 2. Background

2.1 Colloidal particle interactions

2.1.1 Introduction

A knowledge of colloidal particle interactions in suspension is important to understand a wide range of particle/suspension problem because the extent of particle/particle and particle/medium interactions determines suspension behavior such as sedimentation, flow properties including rheological properties, particle stability in the medium (aggregation) and various other phenomena. The results from the inter-particle interactions are usually key to a wide range of industrial process.

2.1.2 Inter-particle interaction forces

The characteristics of a particle suspension are a manifestation of the interaction between particles. Each particle may have an attractive or repulsive force. The degree of inter-particle interaction is governed by the total sum of interaction forces of each of the components. Attractive forces arise from van der Waals, electrostatic attractive (between oppositely charged surfaces), hydrophobic, bridging, and depletion forces (Johnson et al. 2000). On the other hands, repulsive forces come from electrostatic repulsive (between similar charged surfaces), steric hindrance, and hydration. The range and magnitude of each of the forces are controlled by the particle surface chemistry, suspending medium and the presence of chemical additives. For particles in the sub-micron size range, the effect of inter-

particle forces has more important role due to the inherent large surface area.

2.1.2.1 van der Waals attractive force

The attractive forces between particles, which are electrical in nature, were postulated by van der Waals to originate from three sources. First was that attraction may result from two interacting polar molecules by virtue of dipole-dipole interactions. Second, polar molecules induce a dipole in neighboring non-polar molecules and this will cause an attraction. The last case is attractive forces that are present between non-polar molecules. An instantaneous dipole moment arises at the instance of uneven distribution of electrons that creates partially negative charge on the side that has more electrons. The instantaneous dipole then induces a dipole on a neighboring molecule. The alignment of the dipole leads to an attraction between two molecules. The effect of the resulting attraction is known as the dispersion or London force.

These forces are a function of separation distance in manner of conveniently expression in terms of the total potential energy of interaction. Hence, increasing the distance between particles reduces the potential energy. The attraction potential, V_A, between two colloidal particles is estimated by integrating the interaction between atoms in each particle. The integration is carried out by assuming two colloidal particles exist as two infinitely large flat plates such that:

$$V_A = -\frac{A_H}{12\pi D^2} \tag{2.1}$$

where A_H is the Hamaker constant and D is the distance between two parallel surfaces. The value of A represents a cluster of constants $(\rho N_A/M)^2\pi^2 B$ and is a property of the molecule where $\rho N_A/M$ is in the number of atoms per cubic centimeter and B is polarizing ability of the atom.

The range of interactions between particles as shown in equation 2.1 is longer compared to interactions between two atoms, which are of order a nan0meter or less. This is because the sum of interactions between many atoms from one particle to other atoms on other particle is additive and the effect is known as the 'long-range van der Waals force' or Hamaker force (Hunter 1993).

In case of two equal spheres interacting over a small distance (H=*ca.* 10nm to 20nm), an estimate of the attractive potential is,

$$V_A = -\frac{A_H a}{12\pi H} \tag{2.2}$$

where a is the radius of a sphere and H is the shortest distance between the spheres.

2.1.2.2 Electro-static forces

The interaction between particles that are electro-static in nature can be repulsive or attractive depending on the interacting surface charges. Repulsion will result from interaction between similar charged particles. On the other hand, attraction will arise from interaction between oppositely charged surfaces of particles.

A surface charge on the surface of most substances is acquired when in

contact with a polar (aqueous) medium. The charging mechanisms might come from a range of effects, for example ionization, ion adsorption and ion dissolution. Ionization is established when some particles have surface groups like –OH, -COOH, and NH_2. The ionization of these groups depends strongly on the pH of the solution to provide stabilizing charges; commonly the groups will have negative charge at high pH and vice versa. In case of metal oxides, their surfaces acquire a charge when immersed in water by virtue of unequal adsorption of oppositely charged ions. The metal hydroxide layer reacts with hydroxide ions, OH^- or hydrogen ions, H^+, such that,

$$M\text{-}OH + OH^- \rightarrow M\text{-}O^- + H_2O \quad (2.3)$$

$$M\text{-}OH + H^+ \rightarrow MOH_2^+ \quad (2.4)$$

where M is a metal ion. These reactions are highly pH driven. In ion dissolution, a surface charge for ionic substances depends on unequal dissolution of the oppositely charged ions of which they are composed. This is observed in the case of silver iodide, AgI, particles in an aqueous solution (Shaw 1970).

For a charged particle surface (e.g. a positively charged particle) that moves freely in an aqueous medium, ions of opposite charge (counter-ions) will be attracted and adsorbed to the surface due to an electrostatic interaction. Consequently, the concentration of counter-ions is high and in this example, the local charge now becomes negative. Ions of like charges (co-ions) then compromise the charge until the surface potential, Ψ, decreases and eventually reduces to zero. The unequal distributions of ions

lead to the formation of a diffuse electric double layer (EDL). The characteristics of the electric double layer, such as its potential and thickness, have a significant impact to the way particles interact.

To understand the interaction of the electric double layer, two regions of ion distribution are generally considered. This being an inner region which includes adsorbed ions, and a diffuse region in which ions are distributed according to the influence of electrical forces and random thermal motion.

A schematic form for the EDL has undergone a number of revisions. The surface is assumed flat and uniformly charged, the distribution of ions in the diffuse part are treated like point charges according to the Bolzmann distribution. The influence of the solvent to the layer is through its dielectric constant, and a single symmetrical electrolyte of charge number, *z*, is assumed.

The Posson-Boltzmann equation was applied to describe the potential and ion distribution in an electrolyte solution in the presence of a charged surface. The equation considers the electrostatic potential, Ψ, at any point near the surface, volume charge density, ρ, and electrostatic interaction between ions and the thermal energy, *kT*, such that,

$$\frac{d^2\Psi}{dx^2} = \frac{-1}{\varepsilon_0 \varepsilon_r} \sum_i n_i^o z_i e \exp\left(\frac{-z_i e \Psi}{kT}\right) \tag{2.5}$$

where ε_0 is permittivity of a vacuum, ε_r is the relative permittivity, n_i^o is the number of ions type *i* per unit volume in the bulk solution far from the surface, z_i is the ion valance, *k* is the Boltzmann constant, *T* is the temperature and *x* is the distance from the surface. Assuming the electrical

energy is smaller than the thermal energy of the ions such that $(|z_i e\Psi| < kT)$, equation 2.5 is then reduced to

$$\frac{d^2\Psi}{dx^2} = \left(\frac{\sum -z_i^2 e^2 n_i^0}{e_w kT}\right)\Psi = \kappa^2\Psi \tag{2.6}$$

where $\kappa = \left(\frac{e^2 \sum -z_i^2 n_i^0}{ekT}\right)^{\frac{1}{2}}$ (2.7)

The above linear approximation is called the Debye-Hückle approximation and successfully predicts the exponential decay of the potential of the double layer in the form of

$$\Psi = \Psi_0 \exp(-\kappa x) \tag{2.8}$$

where Ψ_0 is the surface potential, x is the distance from the surface, and κ is called the Debye-Hückle parameter. The inverse of κ, (κ^{-1}), is generally known as the thickness of the double layer or Debye length.

A more realistic approach has been resolved by combining the previous model. This new model involves a compact inner region very close to the surface followed by a diffuse layer of ions. The inner layer is suggested to consist of a fixed finite size ion counter-ion specifically adsorbed to the surface. The centers of the adsorbed ions are located in the Stern plane. Ions located beyond the Stern plane are considered to be in the diffuse part of the double layer. The compact layer is treated as a series of miniature capacitors in order to calculate the potential drop which decays from Ψ_δ (Stern potential) to zero in the diffuse double layer. The Stern potential Ψ_δ is a useful reference point in terms of colloidal interactions. It is often estimated

from the potential measured using electrokinetic techniques such as electrophoresis. The potential, often called zeta (ζ)-pontential measures potential at the surface of shear between the charged surface to the electrolyte solution. The net charge on the surface of particles does not always depend on the nature of the surface charge. Ions or charged molecules may attract and adsorb strongly to the surface. This can reduce or alter the effective charge of the particle. In this case, the measurement of ζ-pontential is useful in that it is a measure of the interaction potential.

The calculation for the repulsive energy of interaction for a particle with the overlap of the double layer is complex. The calculation is generally performed by treating the simplest case: interaction between a pair of large particles with thin double layers. In the case of $\kappa a >> 1$ (where a is the particle radius), the double layer interaction can be treated similar to that for flat plates. When the double layer begins to overlap, an osmotic pressure develops due to the accumulation of ions within the gap. If the particles approach each other slowly enough, the charges on the plate will be neutralized by counter-ions in order to maintain equilibrium and hence create repulsive force that oppose the plated from moving closer (Hunter 1993).

The overlap of the double layers can be investigated in two conditions. First, the surface potential that is assumed to remain fixed at Ψ_δ (the surface potential the plane where the diffuse layer begins, at $x=d$) as the particles approach, which means the surface charge must gradually discharge in order to maintain constant potential. Second, the surface charge is assumed to remain constant and it is the surface potential that changes. The interaction

energy of identical spheres under both constant potential and constant charge conditions respectively is given by Hunter (1987):

$$V_R^{\Psi} = 2\pi\varepsilon a\Psi_d^2 \ln(1 + exp[-\kappa H]) \quad (2.9)$$

$$V_R^{\sigma} = -2\pi\varepsilon a\Psi_d^2 \ln(1 - exp[-\kappa H]) \quad (2.10)$$

where H is the inter-particle separation distance. These equations are derived assuming the Debye- Hückle approximation (for the case of low surface potential) and the double layer is thin compared to the particle size. In a situation where the overlap of the electrical double layer is small ($e^{-\kappa H} \ll 1$), then both expressions reduce to:

$$V_R = 2\pi\varepsilon a\Psi_d^2 \exp(-\kappa H) \quad (2.11)$$

The total interaction between particles is a combination of attractive and repulsive interaction.

2.2 Shear banding of concentrated suspensions

2.2.1 Shear banding behavior

Shear banding is flow behavior with appearance of the adjacent region of different shear rate. Shear banding behavior is often observed in the flow of soft materials such as wormlike micelle solutions (Fielding and Olmsted 2004; Fielding 2005; Fielding and Olmsted 2006; Fischer et al. 2002; Lerouge et al 2006; Manneville et al 2004; Salmon et al. 2003; Wilson and Fielding 2006; Yesilata et al. 2006), entangled polymers (Remmelgas and Leal 2000; Tapadia and Wang 2004; Tapadia and Wang 2006; Tapadia et al. 2006; Wang 2007), concentrated suspensions (Cohen et al. 2006; Derks et al. 2004; Holmes et al. 2004; Shereda et al. 2010; Wu et al. 2009), foams (Kabla and Debregeas 2003), and liquid crystal (Olmsted and Goldbart 1990). When shear banding occurs instead of simple shear flow in general, the flow becomes complex and flow instability may be involved.

2.2.2 Plateau in flow curve or stress plateau

Shear banding behavior is often reported with plateau or decreasing of flow curve. The flow curve of various micelle solution was exhibited a stress plateau in the shear stress-shear rate curve at a particular stress value (Rehage and Hoffmann 1991; Roux et al. 1993; Cappelaere et al. 1997; Hernandez-Acosta et al. 1999; Holmqvist et al. 2002). In stress plateau region, the stress exhibits remaining almost constant in a certain range of

shear rates. Under controlled shear stress experiments, when shear stress increases progressively, it is observed a large increase of the resulting shear rate around a critical value (τ_c), which rapidly change from a small value to a much larger value associated with the end of the plateau. Various techniques (small angle neutron scattering (SANS), small angle X-ray scattering (SAXS), birefringence, etc.) have been used to study the structural change or transition in wormlike micelle solution exhibiting this stress plateau. In general, the observations led to conclusion that the stress plateau is correlated to with a phase transition, such as the transition between isotropic and nematic phases in wormlike micelles, the coexistence of the lamellar phase and onions in other surfactant mixtures, or the coexistence of different orientational structures (Berret et al. 1994; Ganapathy and Sood 2008; Garcı´a-Sandoval et al. 2012; Hernández-Acosta et al. 1999; Holmqvist et al. 2002; Miller and Rothstein 2007; Partal et al. 2001; Schmitt et al. 1994). In these studies, they reported global information and it could be conceived that the phase transition was progressive in time but approximately homogeneous in the bulk at any given time because measurements concerned the whole materials in a volume across the observation geometry.

However, in the research with flow birefringence experiments on wormlike micelle solution, it was reported that this transition occurred in space (Cappelaere et al. 1997). In this study, the second phase appears at the first critical shear rate (small value in plateau) and progressively invades the gap as the apparent shear rate increases until it completely occupied the gap

for the apparent shear rate equals the second critical shear rate (larger value in plateau). It may be refered to this effect as shear banding. This phenomenon is different from the heterogeneity of the shear rate distribution, possibly with some unsheared regions, which naturally develops in yield stress flows.

After this study, many studies focusing on the velocity field within flows of various soft jammed systems including concentrated suspension, emulsion, foam, entangled polymer and wormlike micelle solution using different technique such as MRI, light scattering, simple microscopy were reported (Baudez et al. 2004; Bertola et al. 2003; Cohen et al. 2004; Cohen et al. 2006; Derks et al. 2004; Dhont and Briels 2008; Mair and Callaghan 1997; Rodts et al. 2005; Salmon et al. 2003; Tapadia et al. 2006; Wang 2007). All the results show that shear banding develops in the plateau region.

2.2.3 Velocity profile of shear banding behavior in simple shear flow

In contrast with the flow behavior in the case of simple yield stress flows, the consequence of shear banding is a discontinuity in shear rate along the interface between the two regions. In addition, the thickness of one of the bands increases linearly with the apparent shear rate while the shear rate in the sheared region does not change significantly (Coussot et al. 2002; Salmon et al. 2003). In contrast with micelle solution, paste materials including concentrated suspension exhibits apparently no-flow in one of the regions so that shear rate seems to abruptly drop from a finite value to zero

through the interface between the two regions (Coussot 2005; Coussot et al. 2008). In Couette flow, the sheared region is close to the inner cylinder (rotating cylinder). In that case, since the stress decreases with the distance from the axis, the shear rate may significantly vary in the sheared region. As a result, the discontinuity in shear rate at the interface between the sheared and the unsheared regions can be observed only at an appropriate scale depending on the critical shear rate.

The steady state velocity profiles of paste materials showing shear banding seem to be stable over short time periods. But, the unsheared region in steady state exhibited increasing tendency with solid concentration and time of rest before applying shear (figure 2.2.3.1). As considered that rest time gives the time to reconstruct the microstructure and high solid concentration of suspension make a more jamming structure in general, above tendency means that the region of the unsheared region increases with the degree of jamming of the structure.

Shear banding of concentrated suspension (which is one of paste materials) seems different for micelle solution. The two coexisting regions in case of concentrated suspensions appear to contain two materials of very different mesoscopic structure (Coussot et al. 2002) and shear banding behavior is more complex than the simple, stable shear banding of micelle solution. The shear banding of concentrated suspensions is stable only when averaging the velocity profiles over sufficiently long times, but instantaneous velocity profiles appear to significantly fluctuate around this mean value. In particular, the position of the interface between the two regions significantly

varies in time.

Chapter 3. Experimental methods

3.1 Sample preparation

The concentrated alumina suspension was used as a model fluid. Alumina particles are widely used as the raw material for ceramic products, such as a separator membrane of lithium-ion battery. The physical characteristics of alumina include good thermal/chemical stability, good mechanical properties, and high conductivity, to list a few. The alumina particles used in this study were ceramic grade (>99.99%) alpha-alumina (model name AKP-20, Sumitomo chemical, Japan). The average size of the particle was measured by DLS (Dynamic Light Scattering; Zetasizer Nano ZS, Malvern instruments) and was determined to be about 0.5 micron.

The flow was visualized with alumina suspensions of two different dispersion states. One was coagulated, and the other well-dispersed. For the coagulated system, 25vol% and 40vol% alumina suspension was used at pH 9.5. The IEP (iso electric point) of alumina particle was pH 9.5, at which the particles lose the electrostatic force and the van der Waals force dominates the system. For the well-dispersed system, 25vol%, 40vol%, and 55vol% alumina suspension was used at pH 6.5. The particles have strong electrostatic repulsions at pH 6.5, leading to a stable well-dispersed system. To estimate the electrostatic repulsive forces of the alumina suspension, zeta potential was measured using DLS. The measurement was performed with very dilute alumina suspension (0.01vol%) at both pH 9.5 and pH 6.5 using the Zetasizer Nano (Malvern instruments). The zeta potential of alumina particles at pH 6.5 was +30mV, which means that the repulsive forces prevail

in the system. Because of this electrostatic repulsion, there was no aggregation and it was verified that the precipitation due to gravity did not occur in the time scale of this experiment. The zeta potential at pH 9.5 was -1.4mV, and no significant electrostatic repulsion existed.

The alumina suspension was made using the method given by Johnson et al.(1998). As the microstructure of particulate suspension can be significantly affected by the preparation process (Channell et al. 2000), the alumina suspension was always prepared in the same way as illustrated in the following procedure to maintain accuracy and reliability of the measurements. First, the amount of alumina corresponding to the solid concentration was added to deionized water, and background electrolyte (NaCl) corresponding to 0.01M was added. Using anchor type stirring bar on an overhead stirrer, the solution was mixed until the powder was wetted completely and large agglomerates broke. Next, the pH of the solution was adjusted to under pH 6 using HCl. To reduce the change in concentration of the suspension due to the addition of HCl, high concentration (10 mol/L) HCl was used. After adjusting pH to below 6, the solution was mixed for 20 minutes at 6000 rpm using mechanical homogenizer (T180, IKA), after which the suspension was treated by a sonicator (VCX-500, SONIC) for 10 minutes at 80% of maximum output (~400W, pulse mode). As a probing particle, 0.1 vol% spherical copper particles (8μm, Sigma-Aldrich) were mixed for 20 minutes in a mechanical homogenizer. To inhibit the increase in temperature during the sonication and homogenizing process, the mixing was

performed in a thermostat maintained at 25 degree C. Lastly, the pH of the suspension was adjusted for each system (coagulated suspension and well-dispersed suspension) using HCl and NaOH. For the coagulated suspension, NaOH (10mol/L, 0.1mol/L) was used to adjust the pH to 9.5, which is the IEP. For the well-dispersed suspension, HCl and NaOH were used to adjust the pH to 6.5. The copper particles had strong (-) charge at both pH 6.5 and pH 9.5. Because of the strong electrostatic repulsion from the surface charge, aggregation between copper particles or between copper and alumina particles was not observed. The samples had 24 hours of stabilization process on a roll-mill before being used in the experiments. Before and after measurements, the pH and solid concentration were measured to examine possible drying during the measurements. Before the visualization experiments, it was verified that the alumina suspension with copper particles had the same viscosity with the suspension without copper particles.

In case of Newtonian fluid for verification of modified capillary rheometer, silicone oil was used (kinematic viscosity = 0.001 m^2/s; Shin-Etsu). For flow visualization, 10μm PMMA particles were used as a tracer and mixed with silicone oil for 1 hour using overhead stirrer.

Figure 3.1 shows the viscosity of the two 25vol% alumina suspensions used in this experiment. It was measured using the rate controlled type rotational rheometer (ARES, TA instruments). The geometry used was parallel plate with 50mm diameter. The measurement was performed from the shear rate of $10^{-3}s^{-1}$ to $10^{3}s^{-1}$. To prevent slip and to increase the accuracy of the measurement, a sand paper was attached to both plates.

Both suspensions exhibited shear thinning behavior as shown in figure 1. However, the two suspensions showed a very large difference in viscosity depending on pH and dispersion state. Although they had the same solid content, the viscosity of the coagulated system at pH 9.5 was about two orders of magnitude larger than that at pH 6.5.

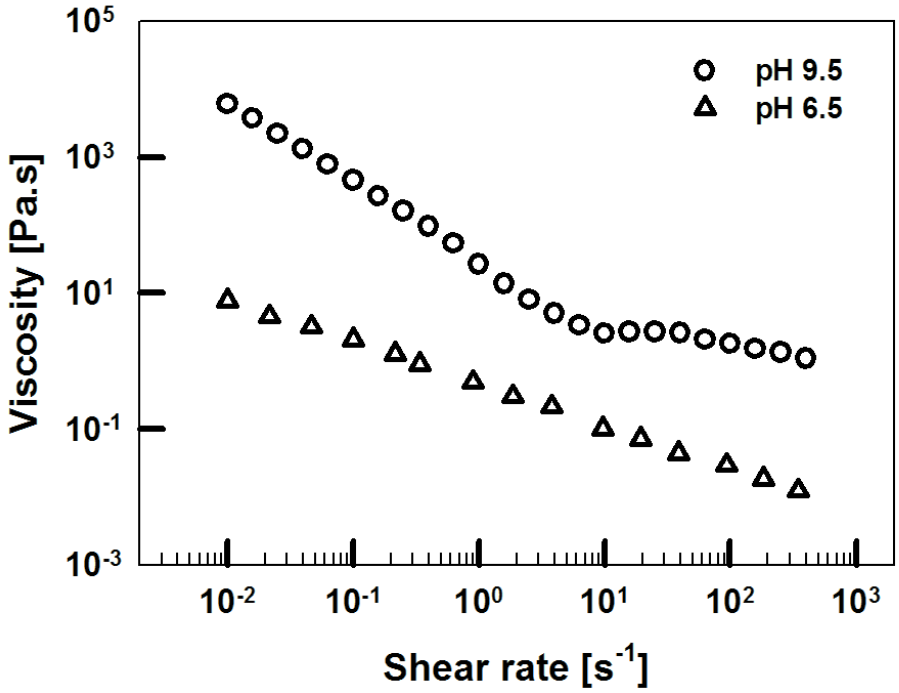

Figure 3.1. Viscosity results of 25vol% alumina suspensions (pH 9.5 coagulated alumina suspension and pH 6.5 well-dispersed alumina suspension)

3.2 Experimental set-up

3.2.1 Modification of conventional capillary rheometer

Capillary rheometer is typically used to measure the rheological properties at high shear rates. It is commonly used to measure the viscosity of highly viscous materials such as polymer melts. The limit of pressure transducer is typically up to 30,000 psi and is not suitable for the suspension systems having relatively low viscosity. Flow visualization is not possible.

To get over these drawbacks, a capillary rheometer (RH7, Malvern Instruments Ltd.) was modified to measure the rheological properties of the suspensions very precisely and reliably from low to high shear rates. At the same time, it was modified to allow *in-situ* flow visualization. New reservoir, extended piston, pressure transducer with high resolution and sensitivity, and a series of capillaries having various aspect ratio and diameter were designed. Simple schematic of modified capillary rheometer is shown in figure 3.2.

The pressure transducer used in modified capillary rheometer has time resolution less than 1 ms and pressure resolution less than 1 Pa. The new reservoir is 300 mm long with a diameter 20 mm, and an extended piston was connected to the original one. Capillary dies having various diameter and length were fabricated for more precise measure. A series of capillary dies having same diameter but different aspect ratio (length) were designed to correct the entrance effect. The diameter of the capillaries was 1mm and the aspect ratios were 2~128 (L/D: 2, 4, 16, 32, 64, and 128).

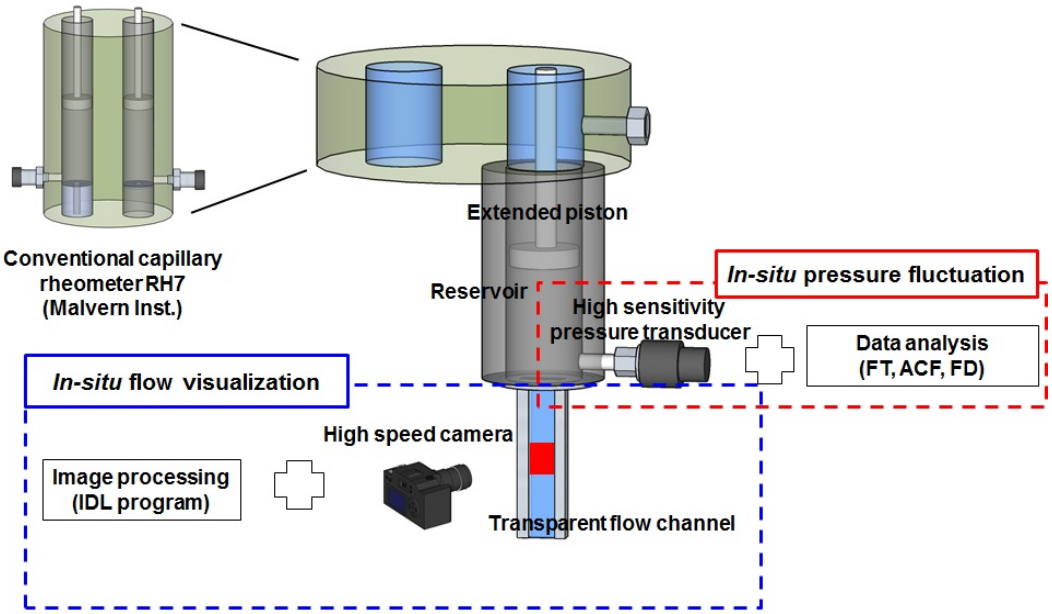

Figure 3.2. Schematics of conventional capillary rheometer RH7, modified capillary rheometer, and flow channel for visualization

Another group of capillaries were designed with the same aspect ratio as 64, but with different diameters to estimate the slip velocity at the wall (D: 0.5mm, 1mm, and 2mm).

The current signals from pressure transducer were converted to rheological variables such as pressure drop or shear stress, which was processed by lab made LabView software. In calculating the viscosity, both Bagley correction (to estimate true shear stress) and Weissenberg-Rabinowitch correction (to estimate true shear rate) were applied.

3.2.2 Flow visualization using modified capillary rheometer

For flow visualization, a transparent slit channel was used. The slit channel made of quartz was combined with metal frame at the bottom of the reservoir instead of metal capillary. Transparent capillary for flow visualization with metal frame is shown in figure 3.3 Three channels having different width (W: 1mm, 5mm, and 10mm) but same depth (H: 1mm) and length (L: 100mm) were used for flow visualization.

The flow was visualized using transparent slit channel and high speed camera. Halogen lamp was used for lightening. Flow visualization was performed with a frame rate 500 fps ~ 2000 fps and shutter speed 1/6,000s ~ 1/2000s, focusing at the center of the slit channel (about 50mm from channel entrance). From the still cut images, the velocity profile of the fluid (more precisely, velocity profile of probe particles) was calculated with IDL (Interactive Data Language) software.

Figure 3.3. Transparent capillary for flow visualization with metal frame equipped to reservoir

IDL program recorded the trajectories of tracer particles for a certain time interval, from which the velocity of tracer particles was calculated.

Procedure of calculating velocity profile in slit channel from still cut images is exhibited in figure 3.4

To visualize the flow of Newtonian fluid (silicone oil), 10㎛ PMMA particles were used as a tracer. The flow was visualized in two slit channels. One was square channel with 1mm (W) x 1mm (H) x 100mm (L) dimension and the other was wide slit channel having 10mm (W) x 1mm (H) x 100mm (L) dimension. The flow was visualized at the center of the channel and depth of focus was 0.5mm (in 1.0mm depth of the channel). The images were taken at 1/2000s shutter speed and 500 fps frame rate. Applied volume flow rate was $30mm^3/s$ and apparent wall shear rate was $30s^{-1}$ for 1mm x 1mm square channel and $3s^{-1}$ for 10mm x 1mm wide channel.

For flow visualization of concentrated alumina suspensions, 0.5wt% 8 micron copper particles were used as a tracer. Solid concentration of alumina suspensions used this study was 25, 40, and 55vol%, respectively. Before visualization experiments, viscosity and other properties of the alumina suspensions were checked with and without trace particles, and no difference was observed.

The flow visualization was performed at constant flow rate mode (rate-controlled), in the shear rate range from $0.1s^{-1}$ to $1,000s^{-1}$. The flows were visualized in a 10mm x 1mm x 100mm (W x H x L) slit channel.

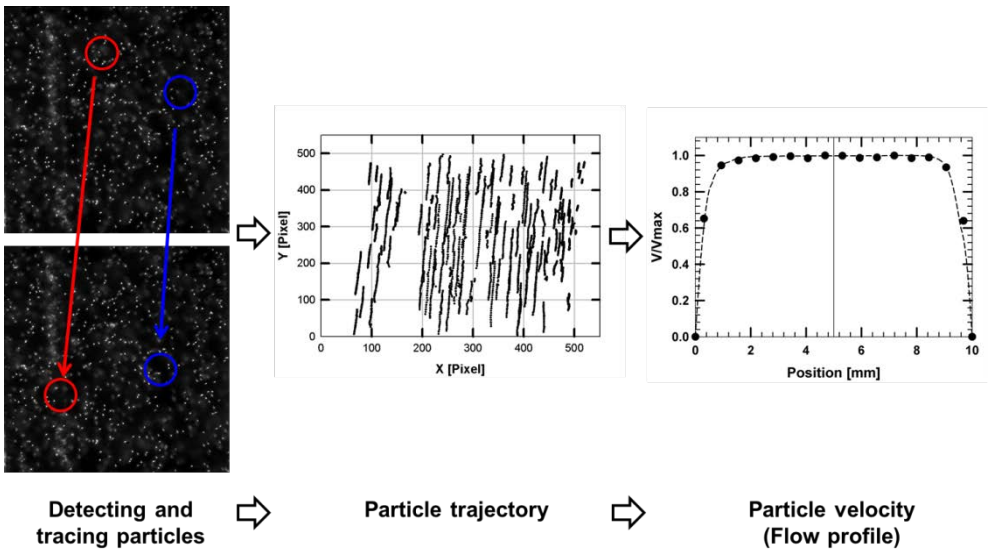

Figure 3.4. Procedure of calculating velocity profile (flow profile) using IDL program

As the concentrated alumina suspension was opaque, it was not possible to trace the particle motion at the center of channel depth (0.5mm deep). In this case, the flow was visualized at 0.15mm depth (30% from channel surface).

Flow profiles by flow visualization were compared to theoretical flow profile of Newtonian fluid. Theoretical flow profile of a Newtonian fluid was calculated by finite difference method in 3D channel having the same dimension used in visualization experiments at the same flow conditions.

3.2.3 Data analysis method for pressure fluctuation

In this study, pressure signal was measured at the same time as flow visualization and analyzed. For this purpose, sensor with high sensitivity, shielding of spurious signal, and smarter data acquisition method were usually supposed. In this study, pressure transducer having high sensitivity was used. The pressure transducer has time resolution less than 1 ms and pressure resolution less than 1 Pa. For reducing noise signal from electronic connection, double shielded BNC-type cables were used in all external electric connection including connection between pressure transducer and DAQ (Data Acquisition) board. The raw data (current signal) from the pressure transducer was recorded by 16bit analog to digital converter (ADC) with a sampling rate up to 100 kHz for one channel. Current signals measured by the transducer (100,000 points per second) were reduced to smaller number of points (100~1000 points per second) using oversampling technique to reduce signal fluctuation or increase signal sensitivity (Dusschoten and Wilhelm 2001). Then the oversampled current signals were

converted to rheological variables such as pressure drop or shear stress, which was processed by lab made LabView software.

Dusschoten and Wilhelm (2001) reported the method for increasing torque transducer sensitivity using oversampling technique. The first step of this method is to acquire the signal at the highest possible acquisition rate as allowed by a high performance ACD card. In the second step, the raw data from first step is truncated on the fly by means of so called “boxcar average” over hundreds or thousands of raw data points. This step is called as “oversampling”. The average is over a fixed number of data points (*N*) between *t* and $t + \Delta t$ that results in a single data point at $t + 0.5\Delta t$:

$$p(\tau_n) = p(t_n + 0.5\Delta t) = \frac{1}{N}\sum_{k=n}^{n+N} T(t_k) \quad (3.1)$$

Where *T(t)* represent the original raw data from the pressure transducer at time *t*, and $p(\tau)$ is the pressure signal after applying the oversampling method. Each of these new values has an inherently lower relative stochastic noise level due to the applied averaging procedure. The applying boxcar average to the raw time data makes a new time domain data set having strongly reduced number of data points and reduced random noise for each new data point (Humberto et al. 2010). The concept of this method was exhibited in figure 3.5 (Humberto et al. 2010). In figure 3.5(a), data in region I represent original data obtained by a conventional transducer, typical sampling rate of $2.5X10^0$ point/s and data in region II exhibited oversampled data taken with a scan rate of $3.3X10^4$. In region III, data exhibits oversampled pressure with scan rate of $2.5X10^5$.

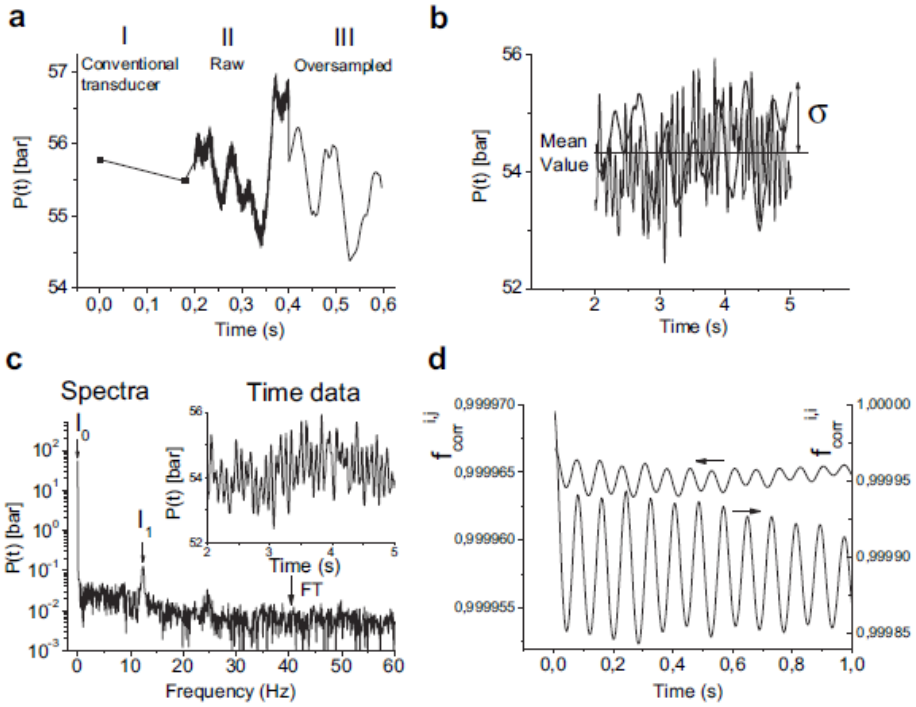

Figure 3.5. Examples of the mathematical framework with various data analysis methods for pressure fluctuation (signal), a) oversampling technique, b) moment analysis for data after oversampling method, c) Fourier transform (FT) spectra of the time-data pressure fluctuation, d) Auto-correlation function (Humberto et al. 2010)

The pressure data after oversampling method was analyzed quantitatively using data analysis method such as Fourier transform (FT) method. A Fourier transform is a mathematical method to quantify the periodic character from a time dependent signal. It exhibits their amplitudes and phases as a function of the frequencies (Hilliou et al 2004; Honerkamp 1994; Wilhelm et al. 1999; Wilhelm 2002). In this way, a complete characterization of experimental periodic functions without loss of any information is achieved. The FT of any real or complex time signal, in case of the pressure p(t), or frequency dependent spectrum $P(\omega)$, is usually defined in the following way:

$$P(\omega) = \frac{1}{\sqrt{2\pi}} \int_0^{+\infty} p(t) e^{-i\omega t} \mathrm{d}t \tag{3.2}$$

$$P(t) = \frac{1}{\sqrt{2\pi}} \int_0^{+\infty} p(\omega) e^{+i\omega t} \mathrm{d}\omega \tag{3.3}$$

where $\omega = 2\pi f$, with f representing the frequency. From equation (3.2) and (3.3), it defines the spectral density function $D_p(\omega)$:

$$D_p(\omega) = \left[\int_0^{+\infty} p(t) e^{-i\omega t} \mathrm{d}t \right]^2 \tag{3.4}$$

In general the Fourier transform is an invertible, linear, and complex mathematical operation. The Fourier spectra $P(\omega)$ have non-zero values only at frequencies $\omega/2\pi$ that are present within the original time dependent function. By using FT analysis it is possible to find parameters that quantify the time dependent signal. Therefore, under flow instability conditions the time dependent pressure data can be described as a sum of different harmonic contributions:

$$p(t) = \bar{p} + \sum_{i \geq 1} I_i \cos(\omega_i t + \emptyset_i) \tag{3.5}$$

where p is the pressure mean value; $\omega_i/2\pi$, φ_i and I_i are the related characteristic frequencies, phases, and amplitudes of the pressure fluctuation as quantified from the Fourier analysis of the processed signals. It is assumed that all the information related with the flow instability is included in these parameters: ω_i, φ_i and, I_i since an FT is an invertible mathematical operation. In the Fourier spectra the intensity at $\frac{\omega}{2\pi} = 0$ is the mean pressure value p of the signal (Humberto et al. 2010). The example of FT results was exhibited in figure 3.5(c).

Chapter 4. Results and Discussion

4.1 Verifying the performance of modified capillary rheometer

4.1.1 Verification of rheological properties

To verify the performance in both flow visualization and viscosity measurement, Newtonian fluid (Silicone oil with kinematic viscosity = 0.001 m^2/s) was tested in advance. The viscosity was measured with the modified capillary rheometer and compared with that measured by rotational rheometers (ARES and AR-G2, TA instruments). And the flow was visualized with PMMA tracer particles, and the flow profile was compared with the one calculated theoretically. Then the viscosity of 55vol% alumina suspension (pH 6.5) was measured and also compared with the one measured by two rotational rheometers (AR-G2, stress controlled; ARES, strain controlled). To measure the viscosity using modified capillary rheometer, both Bagley correction and Rabinowitsch-Wessenberg correction were applied, and metal capillary dies were used.

In figure 4.1(a), the modified capillary rheometer measured the viscosity of silicone oil as 1 Pa.s in shear rate range from $50s^{-1}$ to $50,000s^{-1}$ at 25℃ and confirmed that this fluid kept Newtonian behavior up to very high shear rate. And the result matched well with the data from rotational rheometer (ARES). In figure 4.1(b), in case of 55vol% alumina suspension, it exhibited shear thinning behavior at low shear rate up to a certain shear rate after which shear thickening was observed. Critical shear rate for shear thickening was about $500s^{-1}$.

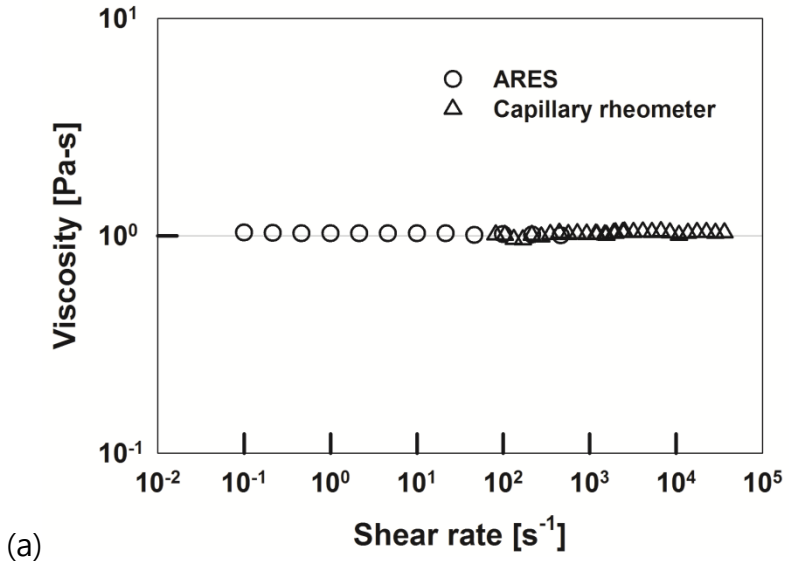

(a)

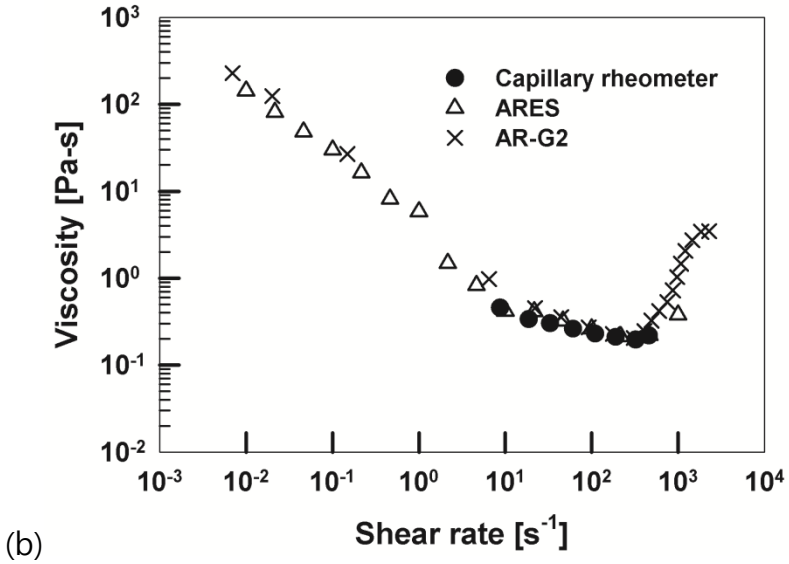

(b)

Figure 4.1. Viscosity results measured by modified capillary rheometer, (a) 1000cS silicone oil, (b) 55vol% alumina suspension

The data matched well for all three different types of rheometers. However, the capillary rheometer could not measure the viscosity in the shear thickening region.

It is because the viscosity of alumina suspension increased rapidly and the suspension responded as a solid in this region. This behavior could be confirmed by a sudden increase of pressure above the critical shear rate.

The pressure measured at shear rate $350s^{-1}$, which is slightly lower than the critical shear rate, was about 3 bar (10% of maximum allowable pressure, 30bar). the pressure measured at shear rate $600s^{-1}$ which is slightly higher than the critical shear rate increased very steeply and reached maximum pressure in a short time. So, the viscosity measurement in this shear rate region was not possible and the strain controlled rotational rheometer showed the same behavior. In general, shear thickening arises when the particles form clusters by hydrodynamic lubrication force, which is not a function of shear rate but a function of shear stress. So, in strain controlled or rate controlled mode of a rotational rheometer, sharp increase in shear stress or large stress fluctuation is exhibited above critical shear rate (Maranzano and Wagner 2001a 2001b). Likewise in our modified capillary rheometer which is operated in rate controlled mode (flow rate controlled), rapid increase in pressure and large pressure fluctuation were observed above critical flow rate (shear rate) and it was hardly possible to get reasonable data in these flow rate region.

4.1.2 Verification of flow visualization

To visualize the flow of silicone oil, 10㎛ PMMA particles were used as a tracer. The flow was visualized in two slit channels. One was square channel with 1mm (W) x 1mm (H) x 100mm (L) dimension and the other was wide slit channel having 10mm (W) x 1mm (H) x 100mm (L) dimension. The flow was visualized at the center of the channel and depth of focus was 0.5mm (in 1.0mm depth of the channel). The images were taken at 1/2000s shutter speed and 500 fps frame rate. Applied volume flow rate was $30mm^3/s$ and apparent wall shear rate was $30s^{-1}$ for 1mm x 1mm square channel and $3s^{-1}$ for 10mm x 1mm wide channel. Theoretical flow profile of a Newtonian fluid was calculated by finite difference method in 3D channel having the same dimension used in visualization experiments at the same flow conditions.

This Newtonian fluid exhibited parabolic flow profile in 1mm x 1mm square channel and plug flow profile in 10mm x 1mm wide channel (Figure 4.2(a) and 4.2(b)). The velocity profile quickly reached steady state upon the start-up of the flow, and the results matched well with the velocity profile that was calculated theoretically. For Newtonian fluid, the modified capillary rheometer could measure the viscosity very precisely up to high shear rate, and the result matched well with that measured with conventional rotational rheometers. Flow visualization also exhibited the same velocity profile as the one calculated theoretically. Based on these results, the performance of the modified capillary rheometer could be verified.

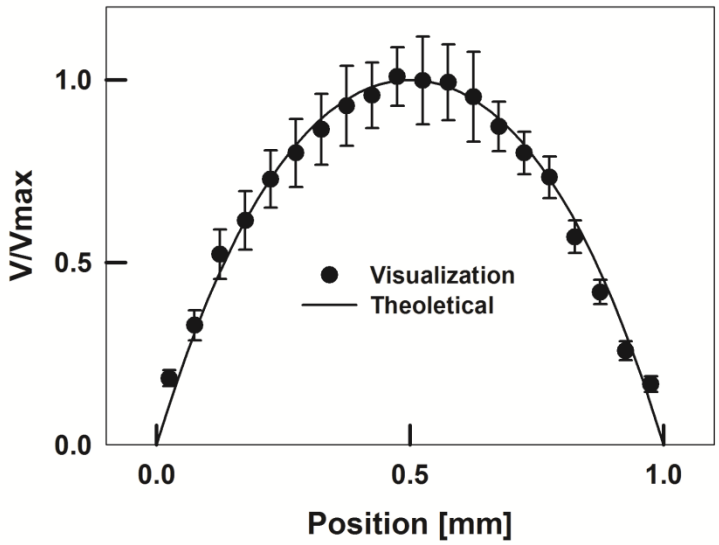

(a)

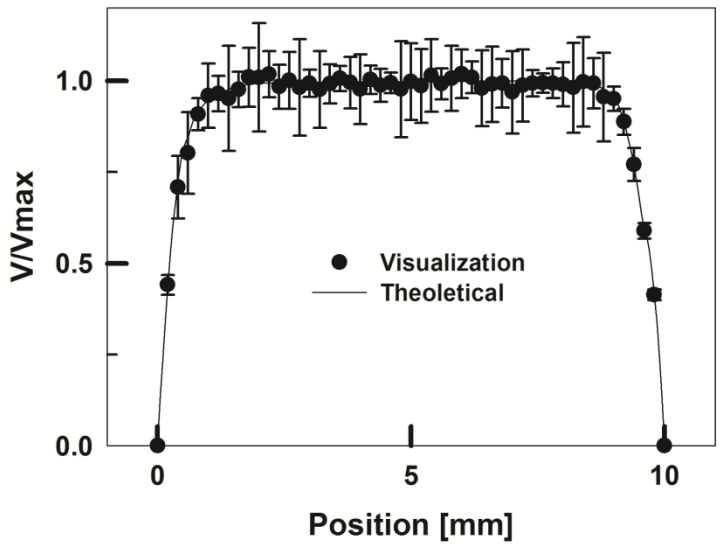

(b)

Figure 4.2. Velocity profile of 1Pa.s silicone oil (Newton fluid), (a) 1mmX1mm, (b) 10mmX1mm

4.2 Flow visualization of well-dispersed alumina suspensions

4.2.1 Transient flow behavior

The flow of 55vol% well-dispersed alumina suspension (at pH 6.5) was first visualized using 10mm x 1mm x 100mm wide slit channel at shear rate $0.3s^{-1}$ which belongs to shear thinning region (Figure 4.3(a)). In figure 4.3(a), the suspension exhibited complicated transient flow behavior in which the flow profile was developed as a function of time, unlike Newtonian fluid in which the flow quickly reached steady state. There was no-flow at first for about six seconds after the start-up (after piston started to move), after which the fluid started to flow only in the center region (3mm~7mm in channel width; about 40% of the whole channel size) at very low speed, while there was no flow near the channel wall. Then the flow region expanded, while the flow rate increased and flat velocity profile was shown up in center region. Up to a certain time (~ 12 s), considerably wide region of no-flow was observed but the regime decreased as time passed. In 12 s after the start-up of flow, it reached seemingly steady state. At this state, it showed symmetric and flat velocity profile in center region, but significantly different flow profile close to the wall from plug-like flow profile as in the case of Newtonian fluid. The velocity profile near the wall was considerably lower than that of Newtonian fluid. Even at (seemingly) steady state, the flow often showed instability such as sudden jamming in which the fluid in some region suddenly stopped and flowed again.

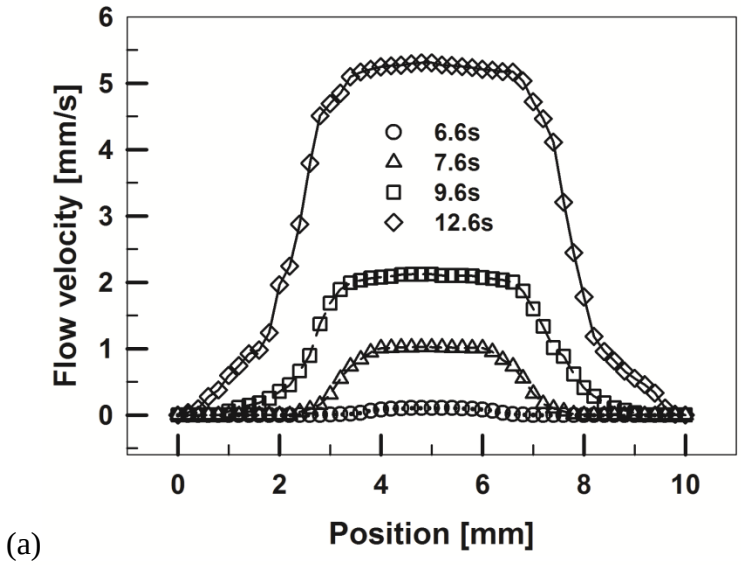

(a)

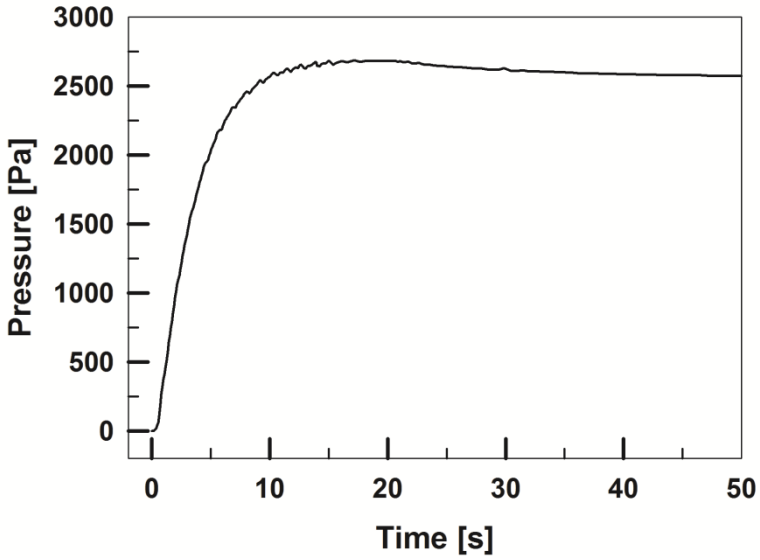

(b)

Figure 4.3. Velocity profile and pressure of 55vol% alumina suspension as a function of time at shear rate $0.3s^{-1}$, (a) velocity profile, (b) pressure profile measured at the same time as flow visualization

In this sense, the flow was meta-stable and did not reach steady state though the overall velocity profile looks steady state in 12 seconds after start-up of the flow.

This transient flow behavior correlates with pressure profile which was measured at the same time (figure 4.3(b)) The transient flow behavior at this constant flow rate (shear rate $0.3s^{-1}$) could be divided into 3 steps (no-flow, continuous change of flow profile, meta stable state) as mentioned above.

Similar to the flow behavior, the pressure profile could also be divided into 3 steps, and it was correlated well with the flow behavior. First, the pressure increased linearly up to about 6s. After this linear region, the pressure exhibited nonlinear increase up to certain time (~12s). Finally, the pressure reached seemingly steady state in which the pressure exhibited very slight but continuous decrease. In the first step for pressure profile at which pressure increased linearly, the suspension showed no-flow. In the second step, the pressure increased non-linearly and the fluid exhibited transient flow behavior in which the flow profile changed continuously from no-flow to meta stable state. When the pressure reached seemingly steady state with very slight decrease, steady flow (sometimes) with irregular flow instability was observed.

This pressure profile is similar to the profile of shear stress when yield stress is measured with vane method (Jonhson et al. 2000). When the shear stress is measured at low shear rate, the shear stress increased linearly at first. After that, the shear stress increased nonlinearly up to a maximum stress and reduced to the steady value. In the region where the shear stress increased

linearly, the fluid exhibited solid-like behavior. In the region where shear stress increased nonlinearly up to the maximum point, the fluid experienced solid-liquid transition and became liquid after maximum stress (often called as a yield stress). Similar to this behavior, concentrated alumina suspension showed no-flow in the region where the pressure increased linearly. After this region, the suspension showed transient flow behavior in which the fluid exhibited transition from no-flow to flow with nonlinear increase in pressure, and finally meta-stable flow with steady pressure profile.

It was reported that the concentrated suspensions often show discrete yielding behavior in which nonhomogeneous flow field is induced with the change of flow field, rather than simple yielding in which homogeneous flow field is developed up to a critical value in the solid-liquid transition region in simple shear flow (Coussot 2005). For concentrated alumina suspensions in slit channel flow, the suspension showed shear banded profile with no-flow region at first and change of flow profile. It looks similar to discrete yielding behavior of concentrated suspension in simple shear flow reported by Coussot (2005). Accordingly, the flow in figure 3 would be thought of as complex yielding behavior or complex solid-liquid transition of concentrated particle suspensions in slit channel flow.

4.2.2 Steady state flow behavior

The flow of 55vol% well-dispersed alumina suspension was also visualized at different shear rates $0.3s^{-1}$, $3.0s^{-1}$, $30s^{-1}$, $300s^{-1}$ in wide slit channel (10mm x 1mm x 100mm) and the flow profiles are shown in figure

4.4. The shear rates all belong to shear thinning region and the results were compared with the flow profile of Newtonian fluid that was calculated theoretically. As the focal depth was 0.15mm from the channel surface (the focal depth was 0.5mm for transparent silicon oil), the velocity profile of the Newtonian fluid was calculated at the same position. Calculated velocity profile of the Newtonian fluid was plug flow regardless of the depth of the channel, but the maximum velocity or plateau velocity increased as the focal depth moved from channel surface to center (0.5mm). However, normalized flow profiles (normalized with maximum velocity) exhibited the same shape at all location of channel depth. The velocity profile of a Newtonian fluid in channel flow was plug shape, in which the velocity plateau exists in the center region of the channel (covering 80% of the channel width) and steep decrease in velocity was observed near the channel wall. The profile was independent of shear rate, and normalized flow profiles were the same at all shear rates.

At shear rate $3.0s^{-1}$, $30s^{-1}$ and $300s^{-1}$, 55vol% alumina suspension showed similar transient behavior as in figure 4.3(a). The flow was stagnant at first, and started to flow at low velocity with no-flow region near the wall, and then the flow region expanded to the full dimension of the channel. The time to reach steady state decreased as shear rate increased. The suspension exhibited symmetric flow profile at all shear rates ($0.3s^{-1}$, $3.0s^{-1}$, $30s^{-1}$, and $300s^{-1}$).

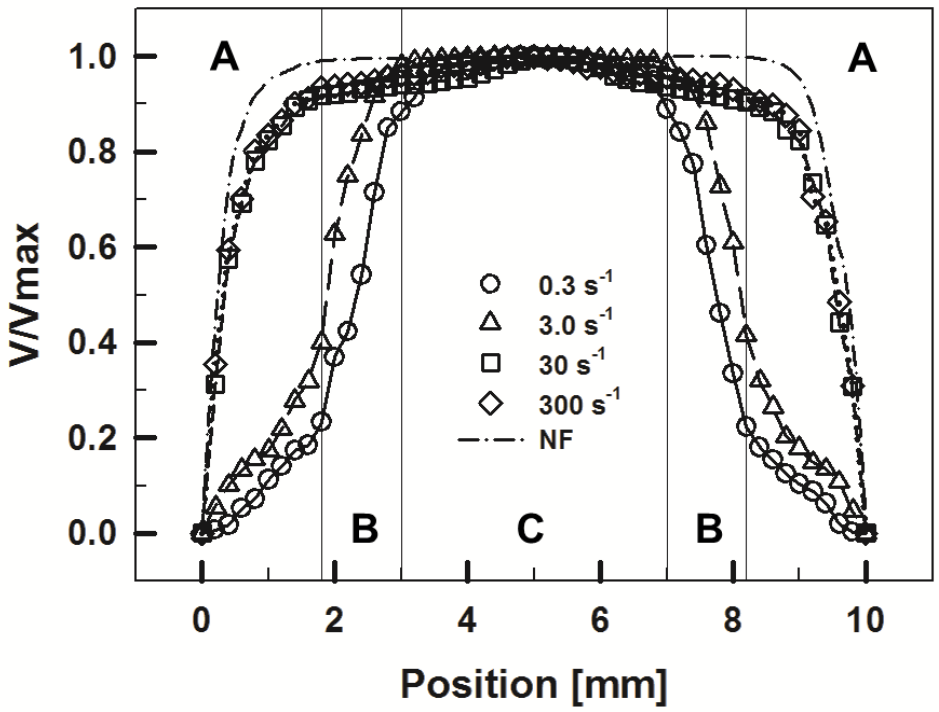

Figure 4.4. Velocity profiles of 55vol% alumina suspension in steady state at shear rate $0.3s^{-1}$, $3.0s^{-1}$, $30s^{-1}$, $300s^{-1}$ and theoretical velocity profile of Newtonian fluid (NF in legend), A, B, and C exhibit regions which are located near the channel wall(0~1.5mm from the wall), in 1.5~3.2mm from the wall, and in 3.2~5.0mm, respectively

However, the flow profile was different depending on shear rate. In particular, the flow at low shear rates ($0.3s^{-1}$ and $3.0s^{-1}$) showed substantially different flow profile than Newtonian fluid while the flow at higher shear rates ($30s^{-1}$ and $300s^{-1}$) exhibited plug –like flow profile similar to Newtonian fluid. The flow profile at low shear rates ($0.3s^{-1}$ and $3.0s^{-1}$) could be divided into 3 regions from channel wall to center (A, B, C in figure 4.4).

In region A which is near the wall (0~1.5mm from the wall, covering 30% in channel width), the suspension flowed at much lower speed and the slope of the curve was much lower than that of Newtonian fluid. In region B (1.5~3.2mm from the wall), the velocity accelerates to maximum. In region C (3.2mm~5.0mm), the velocity keeps almost the same leading to a plug profile. Overall, the flow pattern of the concentrated alumina suspension was significantly different at low flow rate from that of Newtonian fluid, with banded regions which had two inflection points (at boundaries between region A/B and B/C). For Newtonian fluid the velocity profile shows only one inflection point.

At high shear rates ($30s^{-1}$ and $300s^{-1}$), the flow was plug type and the profile kept almost the same independent of shear rate. A rapid increase of flow rate toward the maximum at center and a slightly lower profile than that of Newtonian fluid in region A. In region B and C, slight increase or plateau at channel center was observed. Overall shape of flow profile at higher shear rate was similar to that of Newtonian fluid but the velocity was slightly lower in almost whole channel dimension. At higher shear rate than the critical shear rate $500s^{-1}$ (onset of shear thickening), the suspension showed

solid-like behavior with the same velocity in the whole channel dimension, in which the fluid did not ‘flow’ but was ‘swept out by the piston’.

In the case of lower vol% well-dispersed system, as shown in figure 4.5, the flow profile exhibited a plug-like flow similar to the Newtonian fluid. The fluid velocity increased rapidly near the channel wall, and then showed a plateau in the center of the channel. That is, there exists a region of high shear rate and a plateau region without an inflection point. The velocity profile exhibited no significant change in shape regardless of shear rate covered in this experiment ($0.1s^{-1}$ to $100s^{-1}$).

The flow profile of 25vol% well-dispersed alumina suspension exhibited a similar form to the plug-like flow of the Newtonian fluid, but showed more unstable character even in the region of constant velocity. As can be seen in figure6, the range of measured velocity (size of the error bar) was large away from the center and decreased approaching the center. As the shear rate increased, the range of measured velocity decreased. However, the trend of the decreasing range from the channel wall to the center remained the same. This trend was different from the calculation and also from the visualization of the Newtonian fluid (1Pa.s silicone oil). In the visualization of the Newtonian fluid, the range of the variation in the plateau region was smaller than the case of 25vol% well-dispersed alumina suspension and did not show any trends depending on the position in the channel and shear rates.

In conclusion, the flow of concentrated alumina suspension in shear thinning region could be divided into two types, plug-like flow and shear banded flow with significantly lower flow rate near the channel wall.

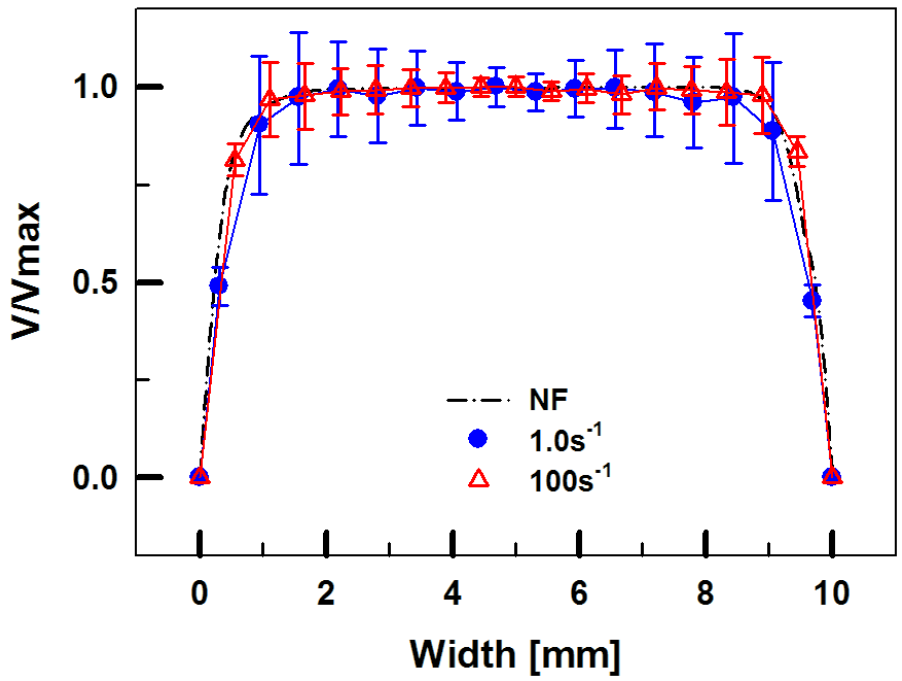

Figure 4.5. Velocity profiles of 25vol% alumina suspensions in steady state at shear rate $1.0s^{-1}$, $100s^{-1}$

The shear banded flow profile could be observed at low shear rate in case of high vol% alumina suspension (55vol%). The plug-like flow was exhibited at high shear rate in case of high vol% suspension and in case of low vol% alumina suspension (25vol%). Shear banded profile was reported in the flow of wormlike micelle solution in slit channel (Fielding 2010; Marín-Santibáñez et al. 2009; Masselon et al. 2008; Yamamoto et al. 2008). In the wide channel, this fluid showed change of flow profile from parabolic shape (Poiseuille-like flow) to plug flow with lower viscosity bands closed to the channel wall (Masselon et al. 2008). In the square channel flow, the fluid exhibited flow profile of parbolic shape in the center region of the channel and region that the micelles are highly oriented along the the flow direction near the channel wall (Marín-Santibáñez et al. 2009). In case of concentrated suspensions, concentrated PMMA suspension showed flow profile which consisted of plug flow in channel center region and region with steep increase of flow rate near the channel wall (Isa et al. 2007). This flow profile was similar with flow profile of concentrated alumina suspension showed in figure 4.4 (shear rate $30s^{-1}$ and $300s^{-1}$) and figure 4.5 These results look similar to our result in that flow profiles could be divided into two types, flow in center region of the channel and region near the channel wall. But the transient flow behavior is much different. The sluggish increase in velocity (region B in figure 4.4) looks unique and has never been reported. In addition, the concentrated alumina suspension exhibited more complex flow profile which has two inflection points.

4.2.3 Correlation between flow behavior and shear stress behavior

In the shear rate range in which wormlike micelle solution showed shear banded flow (Marín-Santibáñez et al. 2009), the stress remained almost constant even when the shear rate increased, exhibiting stress plateau region. It is clear that such a flow behavior is correlated with the stress development in the flow curve (shear stress vs. shear rate). Different flow profile from Newtonian fluid could be observed only in stress plateau region. In other regions where the stress increased monotonically, the flow profile was always Newtonian-like. Therefore, to analyze the unique flow behavior of concentrated alumina suspension, shear stress was measured using rate controlled rotational rheometer (ARES, TA instruments) which was operated in the strain control mode similar to the capillary rheometer. The 50mm parallel plate geometry was used with sand paper attached on the plate to eliminate possible wall slip.

In figure 4.6, the stress curve of 55vol% alumina suspension showed a plateau in which shear stress did not increase and remain constant in the shear rate range from $0.1s^{-1}$ to $10s^{-1}$. The shear stress increased monotonically at shear rates higher than $10s^{-1}$. This behavior having stress plateau in certain range of shear rate was similar to that of wormlike micelle solution.

Shear banded flow profile having lower flow rate near the channel wall than Newtonian fluid was observed in the stress plateau region in figure 4.6 (shear rate $0.3s^{-1}$ and $3.0s^{-1}$).

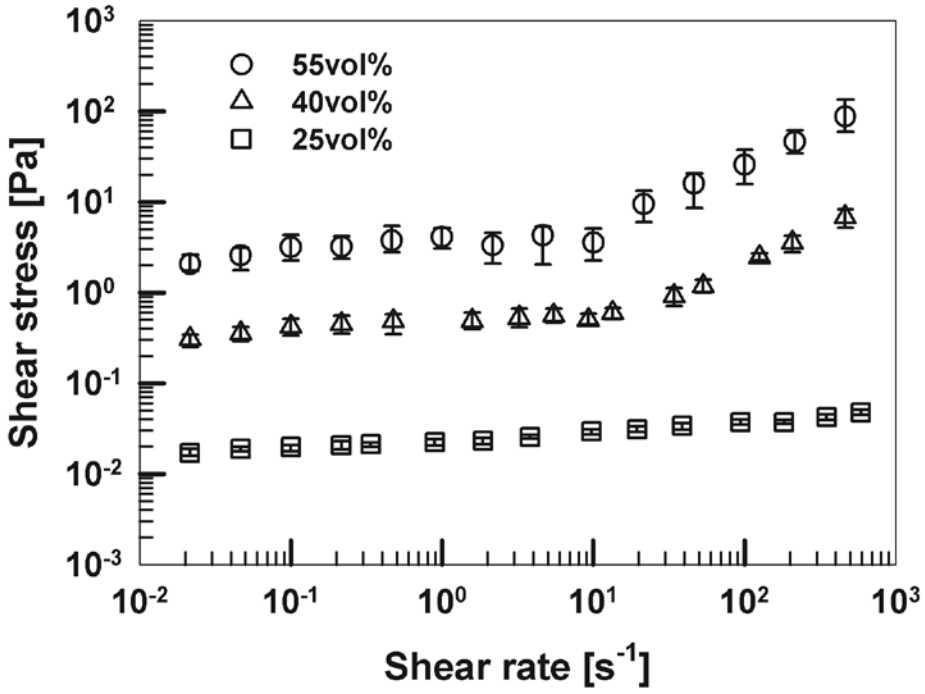

Figure 4.6. Shear stress of alumina suspensions (55vol%, 40vol%, and 25vol%) as a function of shear rate measured by rotational rheometer (ARES)

On the other hand, plug-like flow profile which was similar to Newtonian flow was observed in the region where shear stress increased monotonically with shear rate (shear rate $30s^{-1}$ and $300s^{-1}$). Similar to the case of wormlike micelle solution, the flow behavior of concentrated alumina suspension showed strong correlation with shear stress behavior.

To see more clearly the correlation in the capillary flow, the shear stress of alumina suspensions having the same surface charge (same pH) but with lower concentration (40 vol% and 25 vol%) was measured (figure 4.6). 40vol% alumina suspension showed a stress plateau in the shear rate range from $0.1s^{-1}$ to $10s^{-1}$, after which the stress increased monotonically similarly to the 55vol% alumina suspension. But, in the case of 25vol% alumina suspension, stress plateau was not observed and the stress increased monotonically with shear rate in the whole shear rate region we could cover. To confirm the correlation between stress and flow behavior or the effect of stress plateau on flow profile, two shear rates were chosen and the flows of three alumina suspensions were visualized. One was shear rate $1s^{-1}$ which belonged to the stress plateau region for the two high vol% alumina suspensions, 55vol% and 40vol%. The other was shear rate $100s^{-1}$ which is in the region where shear stress of all three suspensions increased monotonically as a function of shear rate. The results of flow profiles of three alumina suspensions at shear rate $1s^{-1}$ and $100s^{-1}$ are shown in figure 4.7.

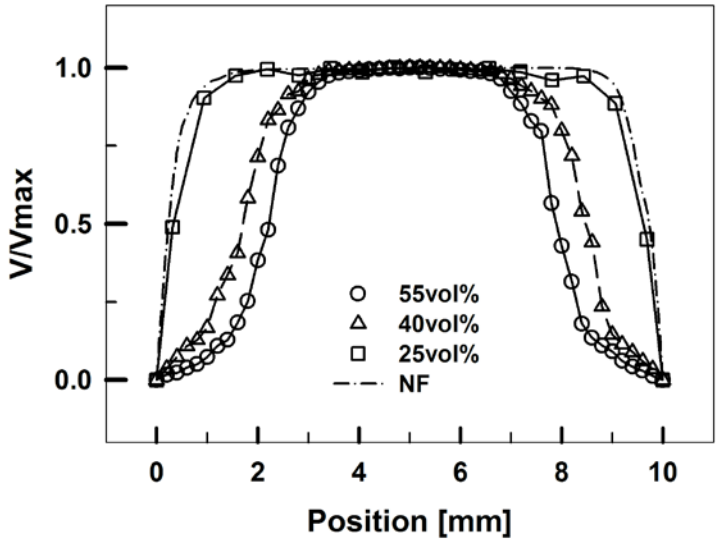

(a)

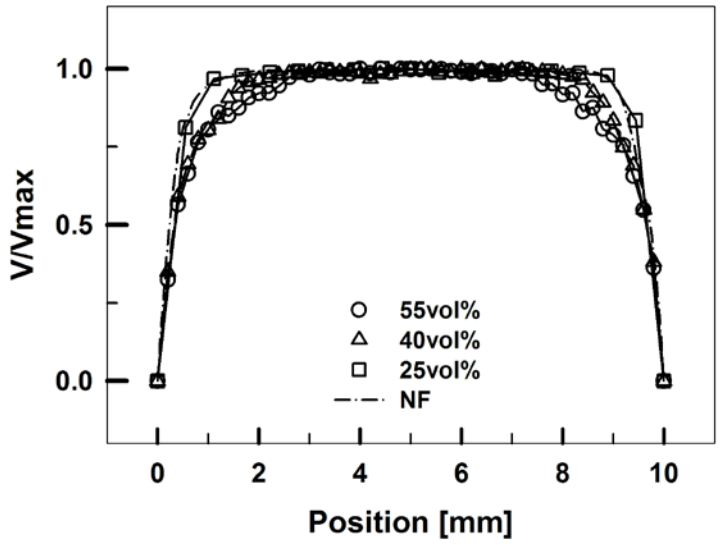

(b)

Figure 4.7. Velocity profile of alumina suspensions (55vol%, 40vol%, and 25vol%), (a) shear rate $1s^{-1}$ (stress plateau region), (B) shear rate $100s^{-1}$

In figure 4.7, 55vol% and 40vol% alumina suspensions showed shear banded flow profile at shear rate $1s^{-1}$ which corresponded to the stress plateau. The profile could be divided into 3 regimes as in figure 4.4. In region close to the wall, the flow was very slow. They also exhibited the region that the flow rate increased steeply toward channel center and the region with velocity plateau. However, the deviation from the Newtonian flow was less pronounced for 40vol% alumina suspension though the shape of the flow curve looked qualitatively the same. For 25vol% alumina suspension which showed no stress plateau, the flow was Newtonian with plug flow in center regime of the channel and sheared zone with steep increase of flow rate near the channel wall. This profile was similar to that of 55vol% alumina suspension at higher shear rates ($30s^{-1}$ and $300s^{-1}$) in figure 4.4. On the other hand, at shear rate $100s^{-1}$ in which all three suspensions showed no stress plateau, all suspensions exhibited the same plug flow profile. Based on the results in figure 4.6 and 4.7, it can be argued that the flow behavior of alumina suspension had a strong correlation to the stress profile, and this correlation was independent of solid concentration. In stress plateau region, the flow of concentrated alumina suspension in slit channel exhibited complex and shear banded flow profile which had considerably lower flow rate than Newtonian fluid, with two inflection points near the wall.

On the other hand, the flow at shear rate which was not related with stress plateau showed similar flow profile as in the case of Newtonian fluid.

Shear banding has long been studied and correlated with stress plateau (Azzouzi et al. 2005; Cappelaere et al. 1997; Fernández et al. 2009; Hernández-Acosta et al. 1999). In stress plateau region, the structural transition or coexistence of two structures was expected, which could be the origin of shear banding with non-homogeneous flow field (Berret et al. 1994; Ganapathy and Sood 2008; Garcı´a-Sandoval et al. 2012; Hernández-Acosta et al. 1999; Holmqvist et al. 2002; Miller and Rothstein 2007; Partal et al. 2001; Schmitt et al. 1994). In addition, the flow behavior in stress plateau region was studied with many soft materials including concentrated suspension, emulsion, foam, entangled polymer and wormlike micelle solution (Baudez et al. 2004; Bertola et al. 2003; Cohen et al. 2004; Cohen et al. 2006; Derks et al. 2004; Dhont and Briels 2008; Mair and Callaghan 1997; Rodts et al. 2005; Salmon et al. 2003; Tapadia et al. 2006; Wang 2007). Concentrated alumina suspension exhibited stress plateau region, which could be correlated with the appearance of shear banded flow in slit channel. It showed sluggish flow profile near the wall as in the flow of concentrated silica suspension in Couette flow (Coussot 2005; Coussot et al. 2008). Also this flow behavior was similar to that of micelle solution in slit channel. However, the flow of concentrated alumina suspension in slit channel was more complex and non-homogeneous than other fluids in similar geometry or the Couette flow of similar fluids.

4.3 Flow visualization of coagulated alumina suspensions

4.3.1 Steady state flow behaviors

The flows of 25vol% coagulated alumina suspensions were visualized at steady state. The flow profiles of suspensions were taken at shear rate $0.1s^{-1}$, $1.0s^{-1}$, $10s^{-1}$, $100s^{-1}$ and their velocity profiles in channel are shown in figure 4.8. These results were also compared with the theoretically calculated velocity profile of a Newtonian fluid. The flow profile of the Newtonian fluid was calculated at the same depth (0.15mm from the surface) where the visualization was made in experiments. The flow profile of 25vol% alumina suspension was either very similar to the Newtonian fluid or significantly different depending on the shear rates.

For the coagulated system, the flow profile, although symmetric, was different from the Newtonian fluid. The steady flow profile was different at different shear rates. Especially at low shear rates, the flow profile was significantly different from that of the Newtonian fluid. At shear rate $0.1s^{-1}$, there was a flow only around the channel center (approximately 60% of the channel width) and there was no flow close to the wall. The region where there was no flow decreased as the shear rate increased, so that the flow region expanded towards the channel wall. The flow was characterized by three regions. First, the flow was very slow and the rate of increase in velocity (towards the center) was low near the wall. Second, the velocity increased at high rates towards the center. Lastly, the velocity formed a plateau near the center of the channel.

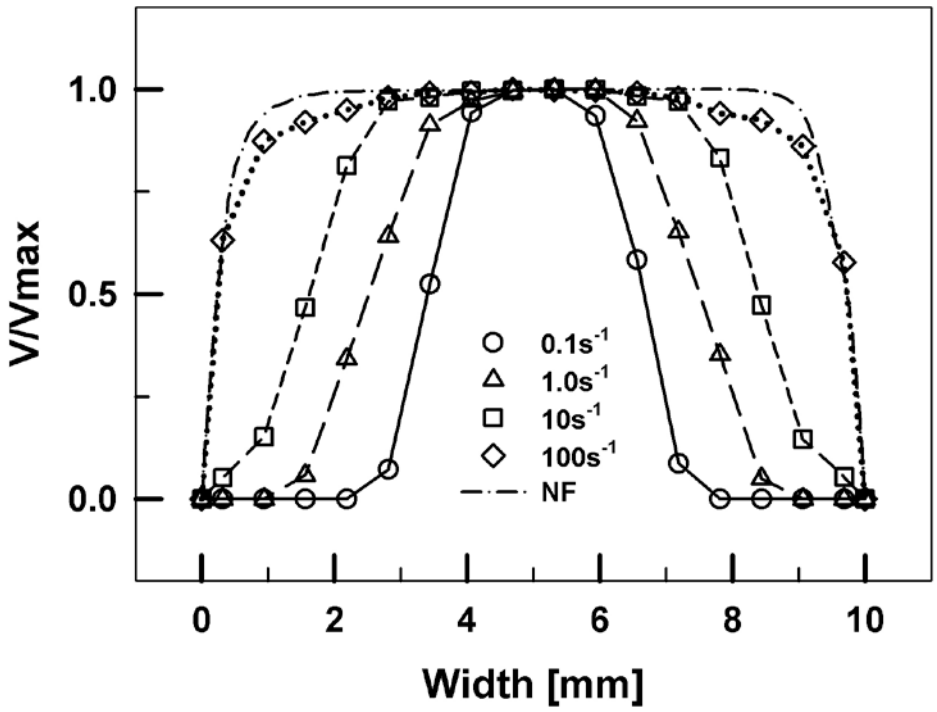

Figure 4.8. Velocity profiles of 25vol% coagulated alumina suspension (pH 9.5) in steady state at shear rate $0.1s^{-1}$, $1.0s^{-1}$, $10s^{-1}$, $100s^{-1}$

This type of flow that exhibited shear banded regions with two inflection points was observed up to a certain shear rate (shear rate of $10s^{-1}$).

At the shear rate of $10s^{-1}$, there was no region where there was no flow, and the flow profile showed shear banded regions with two inflection points. However, at higher shear rates, the regions of low velocity and slow increase in velocity disappeared. The overall flow was similar to the plug-like flow of the Newtonian fluid or that of the well-dispersed suspension.

The shear banded flow profiles of coagulated alumina suspensions in slit-channel was a little different in shape from that in previous studies in which flow profile in slit channel was exhibited as plug-like flow (Fielding and Wilson 2010; Marin-Santibanez et al. 2009; Masselon et al. 2008; Yamamoto et al. 2008). The coagulated 25vol% alumina solution exhibited a more complex flow behavior with two inflection points and significantly lower velocity near the wall.

4.3.2 Correlation between flow behavior and shear stress behavior

Similar to the 25vol% coagulated alumina suspension at pH 9.5, the well-dispersed alumina suspensions with higher solid concentration (55vol% and 40vol%) at pH 6.5 showed shear banded flow profile in our previous chapter 4.2.2. These suspensions showed stress plateau in certain range of shear rates. The shear banded flow profile was observed only in the region of stress plateau. In the region where the stress increased monotonically with the shear rate, the flow profile was plug-like.

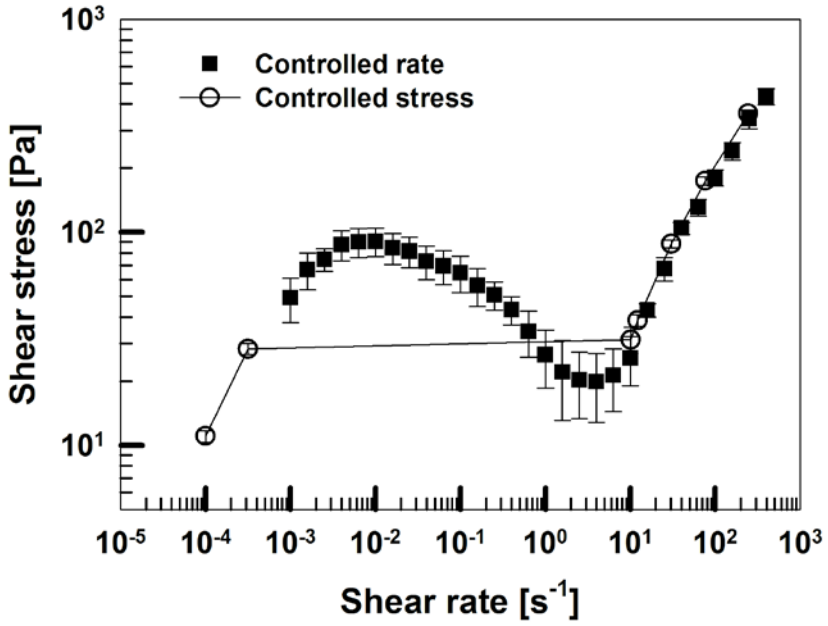

Figure 4.9. Shear stress of 25vol% coagulated alumina suspensions as a function of shear rate measured by rotational rheometer (ARES and AR-G2)

The shear stress was measured as a function of shear rate in order to find the relationship between the shear stress and the flow profile (figure 4.9).

The shear stress was measured using both strain controlled (ARES, TA instruments) and stress controlled rotational rheometer (AR-G2, TA instruments) with parallel plate geometry. For the strain controlled rheometer, the measurement was performed from the shear rate $10^{-3}s^{-1}$ to $10^{3}s^{-1}$. In the case of the stress controlled rheometer, it was performed from the shear stress 10^{-2} Pa to 10^{3} Pa. Each data point corresponds to the average value measured over 60 seconds after conditioning for 180 seconds. To prevent possible slip, sand papers were attached to the plates.

When measured by strain controlled rotational rheometer as shown in Figure 4.9, the shear stress did not increase monotonically with shear rate in certain range of shear rates ($10^{-3}s^{-1}$~$10^{1}s^{-1}$). In this range, the shear stress showed an N-curve with both stress maximum and minimum. On the other hand, when measured by stress controlled rheometer, the shear stress exhibited a “spurt” in the shear rate range mentioned above. When the stress increased slightly, the shear rate increased dramatically from $5*10^{-4}s^{-1}$ to $10s^{-1}$. In the range where the shear rate exhibited the “spurt” from the stress controlled rheometer, the data from the strain controlled rheometer showed a kind of flow instability where the stress decreased with the increase in shear rate. The shear banded flow profile that was shown in figure 4.8 for the coagulated 25vol% alumina suspension was observed at the shear rate in which the shear stress decreased over the shear rate or the spurt was

observed in figure 4.9. On the other hand, the plug-like flow was observed in the region where the shear stress increased monotonically with the shear rate.

4.3.3 Flow development and solid-liquid transition

4.3.3.1 Transient flow behavior

In the coagulated system at high shear rate where the shear stress increased monotonically (shear rate $100s^{-1}$ in figure 4.8), the flow profile was observed to be similar to the plug-like flow of the Newtonian fluid. However, even for this suspension, the flow profile did not reach steady state immediately after the flow was applied as in the case of Newtonian fluid. The suspension exhibited transient behavior of changing flow profile over time. The transient behavior of the suspension at shear rate $100s^{-1}$ is shown in figure 4.10

There was no flow for certain amount of time (12 seconds) after the flow was applied. It began to flow in 12 seconds only in the center of the channel (3~7 mm, about 40% of the channel width), while there was no flow close to the wall. As time passed, the velocity around the channel center increased, and the flow profile became similar to the one at low shear rate in figure 4.8. At this stage, the flow exhibited shear banded profile with sluggish flow near the channel wall and two inflection points. And then, the region of no-flow decreased over time and the flow region expanded toward the channel wall. At shear rate $100s^{-1}$, the suspension reached steady state approximately in 200 seconds after the flow was applied.

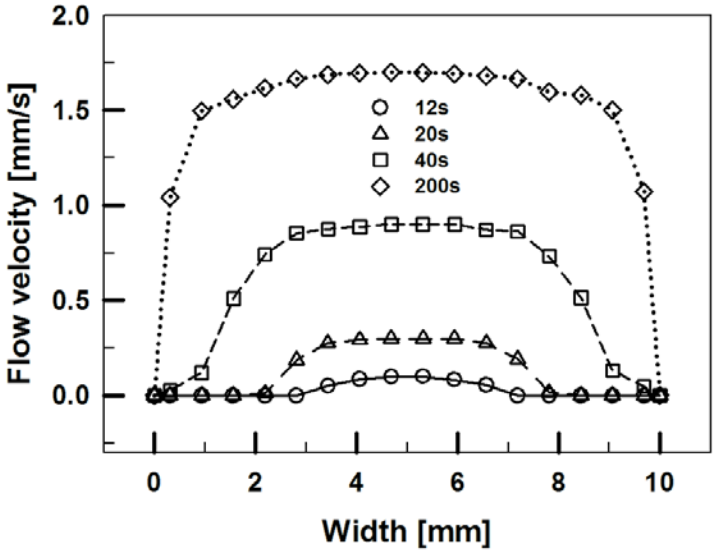

(a)

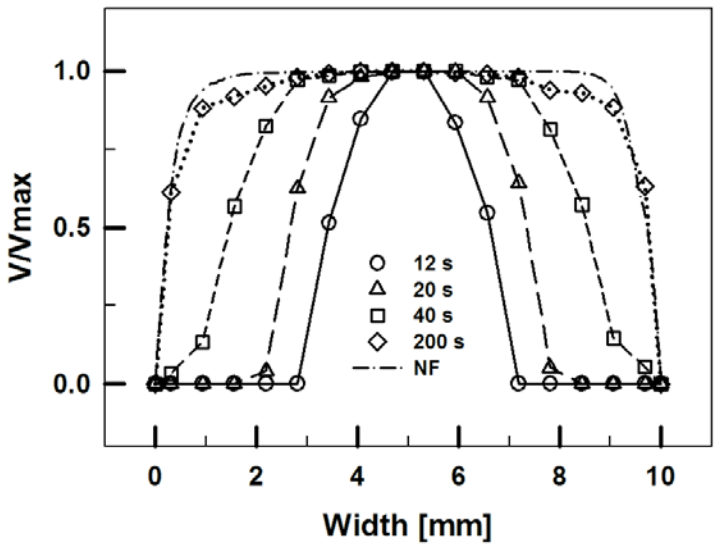

(b)

Figure 4.10. Velocity profiles of pH 9.5 25vol% alumina suspension as a function of time at shear rate $100s^{-1}$, (a) velocity profile, (b) normalized velocity profile of (a)

The velocity profile did not show any significant change afterwards. The transient behavior could be divided into three regions; no-flow, transient flow, and steady flow.

This transient behavior was also found to be related with the pressure profile measured at the same time with the visualization (figure 4.12). The pressure at shear rate $100s^{-1}$ increased linearly for the first 9s, after which the pressure increased non-linearly and reached the maximum value at about 17s. After the maximum, the pressure decreased rapidly up to 60s and reached steady state after 200s. The pressure change over time had a close relationship with the change in flow profile. In the region of linear increase in pressure, the fluid did not flow even after the flow was applied, while the fluid began to flow with wide no-flow region near the channel wall in the region of non-linear increase in pressure. The flow profile after the maximum pressure was shear banded around the channel center and no-flow near the channel wall. In the region of rapid decrease in pressure, the flow profile was shear banded with gradual increase in velocity. In the steady region, the fluid exhibited a steady profile of the plug-like flow.

4.3.3.2 Flow development in solid-liquid transition

The flow profile of a Newtonian fluid and the similar flow profiles of the alumina suspension (the steady flow profile at high shear rate in figure 4.8 and transient profile at 200s in figure 4.10) may well be regarded as liquid-like, while no-flow as solid-like. Then the transient behavior in figure 4.10 demonstrates the solid-liquid transition process.

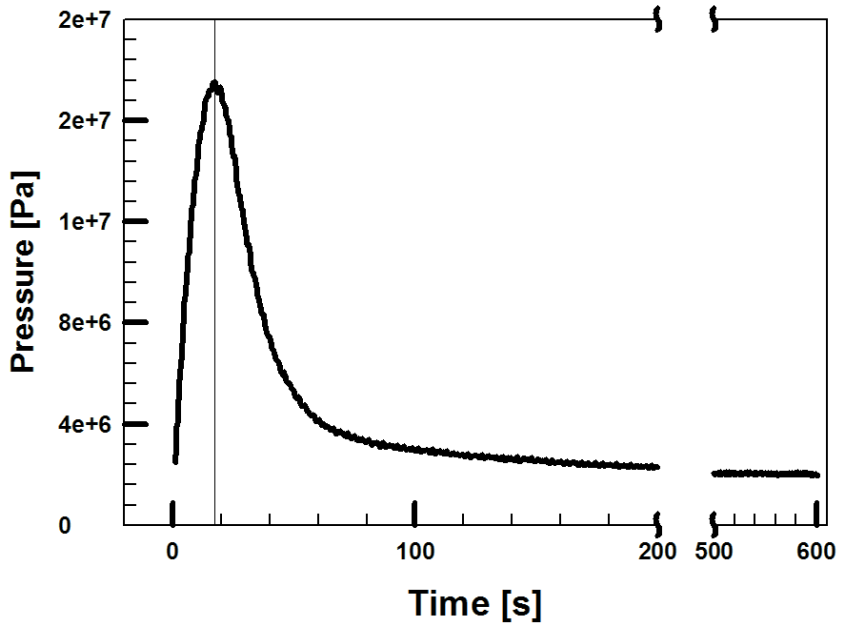

Figure 4.11. Pressure profile of pH 9.5 25vol% alumina suspension as a function of time at shear rate $100s^{-1}$.

The transient flow profile during the solid-liquid transition was shear banded with two inflection points as can be seen in figure 4.10 (~200s). This solid-liquid transition is closely related with the change of flow profile in the stress decrease region in figure 4.9.

The region of stress curve decrease is a type of “discrete” region, in which non-homogeneous flow field is known to be observed. For the reason of stress decay, shear localization (the region of shear is not throughout the dimension but only partial) in the geometry and the expansion of such region has been proposed (Coussot 2005). The region of monotonically increasing stress after this region is a “continuum” region where homogeneous flow field is exhibited. The N-curve in figure 4.9 is a part of the discrete solid-liquid process of coagulated alumina suspension with non-homogeneous flow field and these non-homogeneous flow was exhibited as the form of shear banded flow profile in slit channel flow. In other words, the shear banding in figure 4.8 was a flow pattern that occurred during the discrete solid-liquid transition process in the pressure-driven slit channel flow.

Lastly, it needs to be mentioned that the flow profiles of the transient flow and its trend of change at high shear rate matched well with the steady flow profiles at lower shear rates in the region of stress decrease. Comparing the steady flow profiles with increasing shear rate (figure 4.8) and the transient profiles at high shear rate (figure 4.10(b)), the development of flow profiles in both cases looked similar. At least in this experiment, the transient flow at high shear rate experienced all the steady flow profiles at lower shear rates.

4.3.4 Time periodic pressure fluctuation of coagulated alumina suspension in solid-liquid transition

In the studies of wormlike micelle solutions, the stress plateau was observed in certain range of shear rates. Optical analysis of the shear banding in stress plateau region was reported (Ganapathy and Sood 2008), according to which the shear stress showed a fluctuation with a certain period of time in the plateau region. Such time periodic fluctuation of the shear stress disappeared outside the stress plateau region (in the region of monotonic increase in shear stress) and developed into a chaotic fluctuation. Similarly, the 25vol% coagulated alumina suspension used in this study showed a unique shear banding behavior in the region of stress decrease. The pressure profile was measured in both regions where shear banding occurred and where shear stress increased monotonically, and the results are shown in figure 4.12. The pressure was measured simultaneously with flow visualization. By using oversampling technique, 500,000 points of raw data were converted into 10 points per second (Dusschoten and Wilhelm 2001).

The pressure profile of 25vol% coagulated alumina suspension was fluctuating with a certain time period in the solid-liquid transition as can be seen in figure 4.12(a). The pressure did not reach a steady state. The amount of fluctuation at shear rate $0.1s^{-1}$ was 25%~32% in amplitude with a period of 15.65s (0.064Hz), and 12%~20% in amplitude with a period of 8.3s (0.12Hz) at shear rate $1.0s^{-1}$. Both amplitude and period decreased as the shear rate increased (figure 4.12(b)).

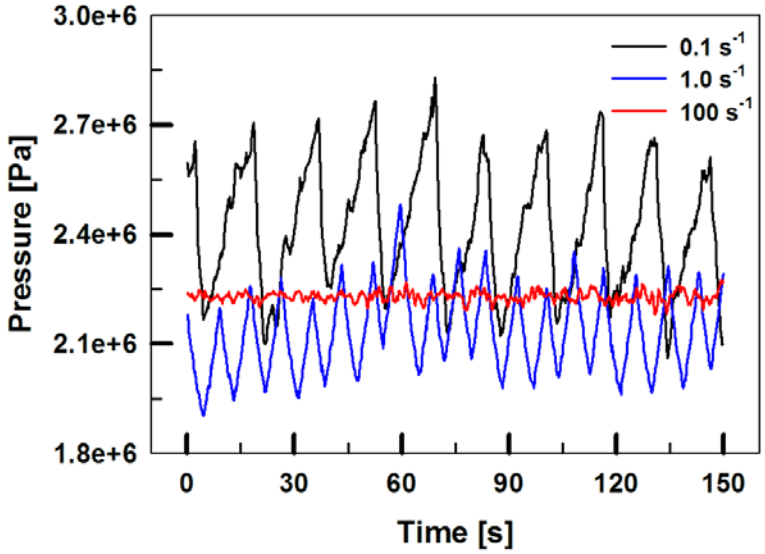
3.0e+6
2.7e+6
2.4e+6
2.1e+6
1.8e+6
Pressure [Pa]
0
30
60
90
120
150
Time [s]
0.1 s-1
1.0 s-1
100 s-1

(a)

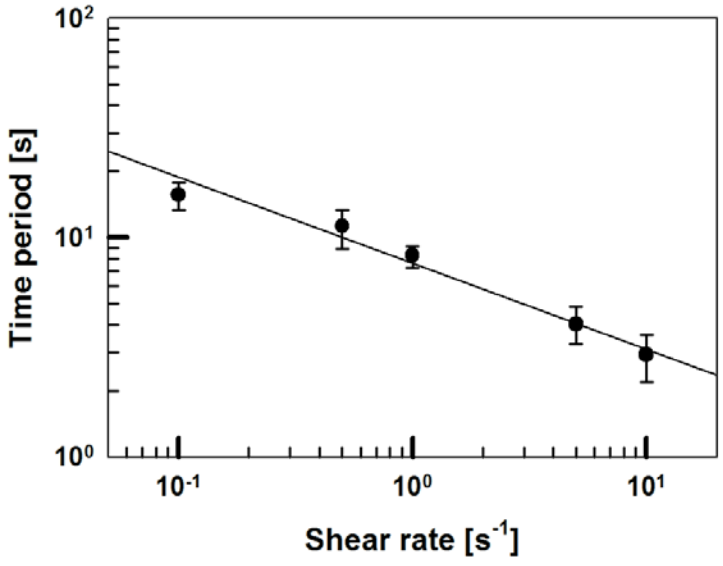
10^2
10^1
10^0
Time period [s]
10^-1
10^0
10^1
Shear rate [s^-1]

(b)

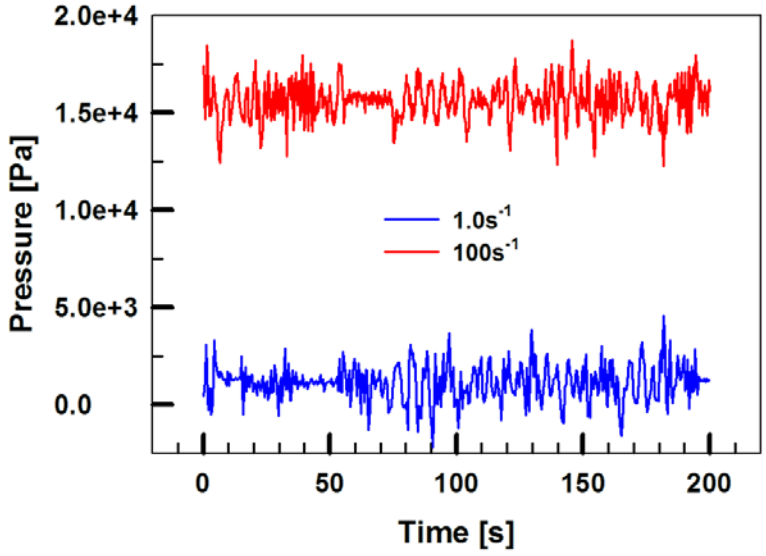

(c)

Figure 4.12. Pressure fluctuation of 25vol% alumina suspensions as a function of time and time periods of pressure fluctuation, (a) pressure fluctuation of pH 9.5 coagulated alumina suspension at shear rate $0.1s^{-1}$, $1.0s^{-1}$, and $100s^{-1}$, (b) time periods of pressure fluctutation of pH 9.5 coagulated alumina suspension in the region of shear stress decrease over increasing shear rate, (c) pressure fluctuation of pH 6.5 well-dispersed alumina suspension at shear rate $1.0s^{-1}$ and $100s^{-1}$

In the liquid region where the shear stress increased monotonically and the flow profile was plug-like, the pressure showed a chaotic fluctuation with no measurable time period. As can be seen in the pressure profile in figure 4.12(a) at shear rate $100s^{-1}$, the pressure exhibited a chaotic fluctuation without a characteristic period. Fourier transformation did not show any characteristic peak. The amplitude of the fluctuation was small with an amount of 1.8%~4%.

For the well-dispersed suspension, only the plug-like flow was observed in the range of shear rates we could cover (figure 4.5). The pressure measurement taken simultaneously with the visualization only exhibited small fluctuation without a certain time period as can be seen in figure 4.12(c). Such a small fluctuation without time periodicity occurred in the same way even at high shear rates.

By observing the development of flow profiles over time and over shear rate together with the pressure profile and the shear stress, it is clear that they are closely related to one another. The flow characteristic during the discrete solid-liquid transition was shear banding (no-flow or sluggish flow near the channel wall with two inflection points). The pressure in this region was not steady but had a time periodic fluctuation. In the liquid region after this transition where the shear stress increased monotonically with shear rate, the flow profile showed a plug-like flow similar to the Newtonian fluid with small pressure fluctuation without a characteristic time period.

4.4 Flow instability of coagulated alumina suspension with high solid concentration

4.4.1 Flow instability in slit channel flow

In the study in chapter 4.3, the flow profile change of coagulated 25vol% alumina suspension during the solid-liquid transition was analyzed. The shear stress behavior at different shear rates, which has a relationship with the flow profile change, was studied, and stress decay in N-curve (differing from the general case of monotonic increase) was observed at certain shear rates. Lastly, in the stress decay region, the coagulated 25vol% alumina suspension exhibited shear-banding phenomenon with the flow profile depicted in figure 4.8.

To understand the complex, non-homogeneous flow profile during the solid-liquid transition better, the stress behavior and the flow profile of 40vol% coagulated alumina suspension, which had high solid concentration, was studied. The shear stress and the viscosity versus shear rate of the pH 9.5 40vol% coagulated alumina suspension are shown in figure 4.13.

As was the case with the coagulated system of pH 9.5 25vol% alumina suspension, pH 9.5 40vol% alumina suspension exhibited shear stress decay over certain regions of shear rate. After this region of decay, the stress monotonically increased.

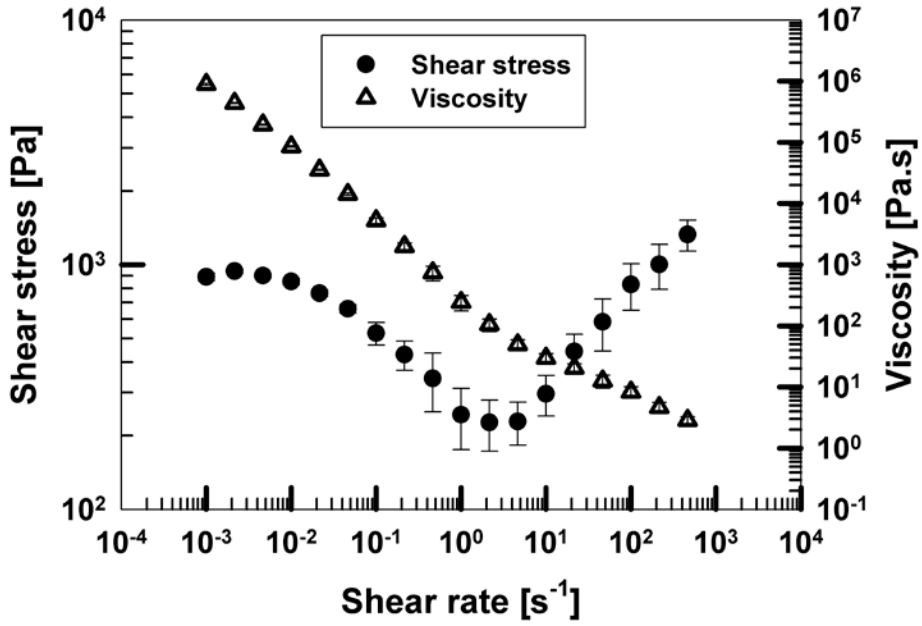

Figure 4.13. Shear stress and viscosity of pH 9.5 40vol% alumina suspension as a function of shear rate measured by ARES with 50mm PP

In general, N-curve behavior of shear stress was observed. Shear stress decayed at the shear rate of $10^{-3}s^{-1}$ to $5s^{-1}$. The shear stress values of 40vol% alumina suspension were higher than that of the 25vol% alumina suspension because of the higher solid concentration. The stress decay region was at a similar shear rate range with the 25vol% suspension.

The velocity profile at the stress decay region of shear rate $0.1s^{-1}$, which is in solid-liquid transition region, and the velocity profile at the monotonic stress increase region of shear rate $100s^{-1}$ are presented in Figure 4.14.

For the case of pH 9.5 25vol% alumina suspension in the stress decay region, the fluid had much lower velocity near the channel wall compared to the Newtonian fluid. It also had a symmetric velocity profile with two inflection points. However, for 40vol% alumina suspension with higher solid concentration, the velocity profile varied significantly over time even at a constant shear rate. The velocity profile did not maintain symmetric form and exhibited asymmetric velocity profile. The no-flow phenomenon was observed in very wide regions. As can be seen in figure 4.14(a2, a3), an extremely asymmetric flow behavior of no-flow region occupying very wide region of one side of the channel wall was observed. In this case, the flow profile in the regions of flow was hard to define and had more complex form than the shear-banded flow.

In the region of monotonically increasing shear stress, flow profile of symmetric plug flow (figure 4.14(b)) was observed, as was the case in the flow profiles of figure 4.8 at shear rate $100s^{-1}$.

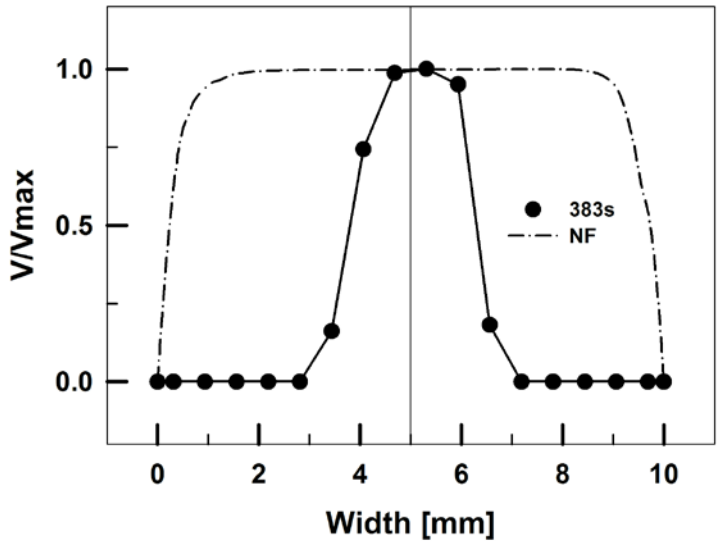
1.0
0.5
0.0
V/Vmax
383s
NF
0
2
4
6
8
10
Width [mm]

(a1)

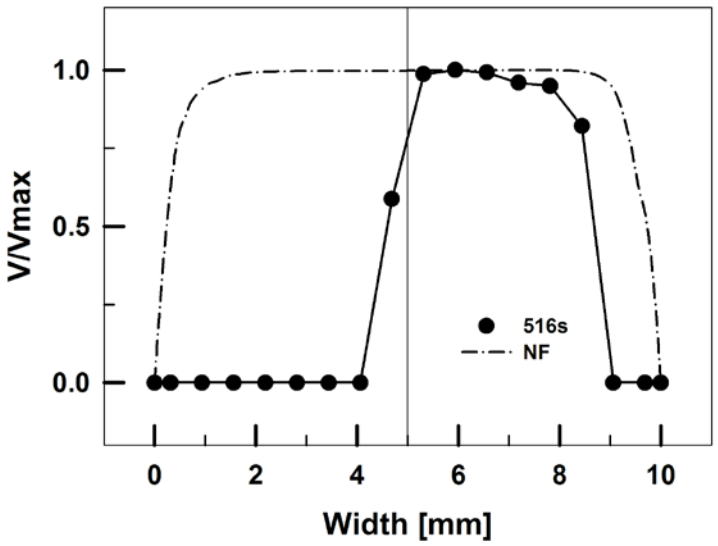
1.0
0.5
0.0
V/Vmax
516s
NF
0
2
4
6
8
10
Width [mm]

(a2)

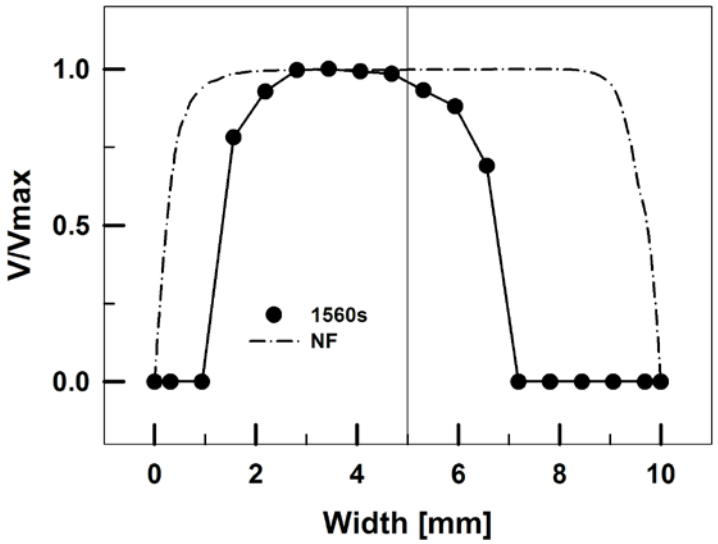
1.0
0.5
0.0
V/Vmax
1560s
NF
0
2
4
6
8
10
Width [mm]

(a3)

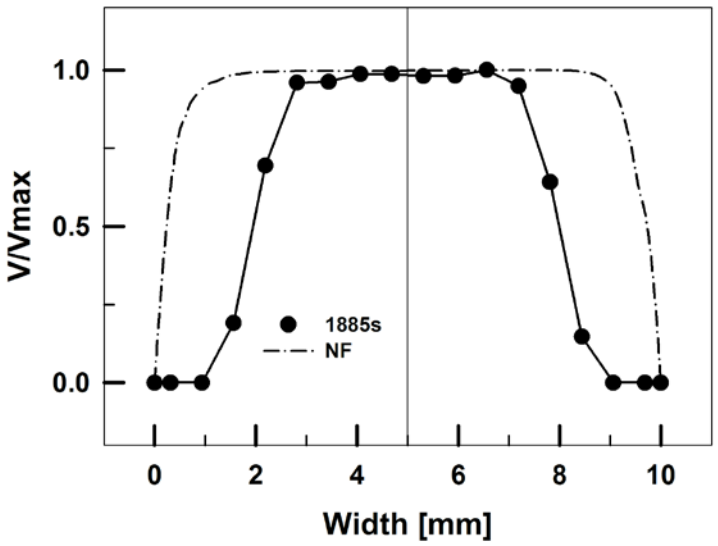
1.0
0.5
0.0
V/Vmax
1885s
NF
0
2
4
6
8
10
Width [mm]

(a4)

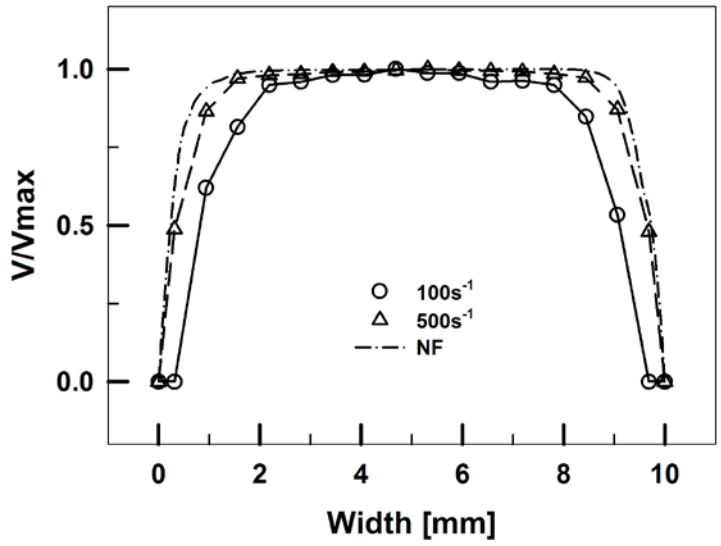

(b)

Figure 4.14. Velocity profile of 40vol% coagulated alumina suspension, (a) velocity profile at shear rate $0.1s^{-1}$ as a function of time, (b) velocity profile at shear rate $100s^{-1}$ and $500s^{-1}$

However, even though it was at the high shear-rate region, no-flow region existed narrowly near the channel wall. After this no-flow region, there was a region of rapid increase in velocity toward the channel center and a separate region of nearly plateau velocity. However, the rate of velocity increase in the region of rapid velocity increase was lower than that of the plug-like flow of Newtonian fluid. The plateau region was also narrower than that of the plug-like flow.

For the higher shear rate of $500s^{-1}$, the flow profile did not exhibit the no-flow region near the channel wall that the flow of shear rate $100s^{-1}$ exhibited.

Another flow characteristic in the stress decay region is that the wide no-flow region does not change irregularly. The no-flow region oscillates sideways with a time period of a few seconds to a few hundred seconds. The flow region's width also was observed to oscillate with a time period of a few seconds to a few hundred seconds.

In order to analyze this time periodic change of velocity profile and the no-flow region, the flow region's width boundary was traced over time, depicted in figure 4.15. The location of the analyzed boundary is and the analysis and time between each analysis was 0.01s. The change in boundary was recorded only when the change exceeded 2pixel (0.04mm) of the 512 total pixels. Figure 4.15(a) is a graph representing the change in the flow boundary width and the flow boundary near the channel wall over time.

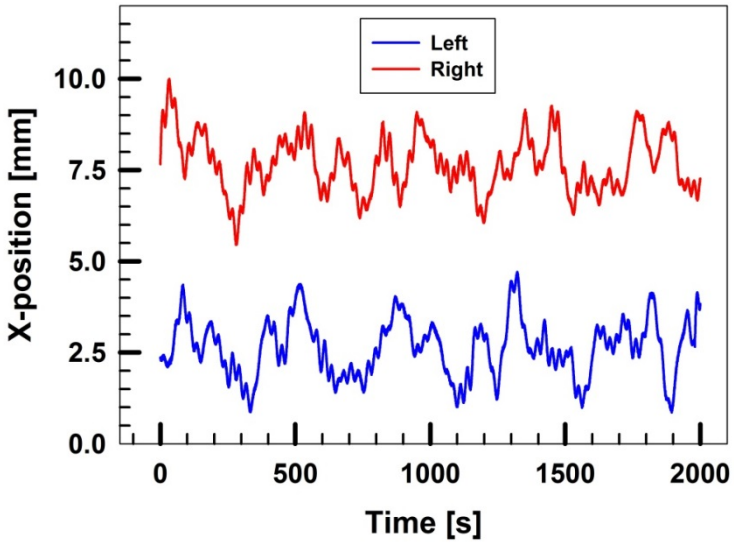
Left
Right
X-position [mm]
10.0
7.5
5.0
2.5
0.0
0
500
1000
1500
2000
Time [s]

(a)

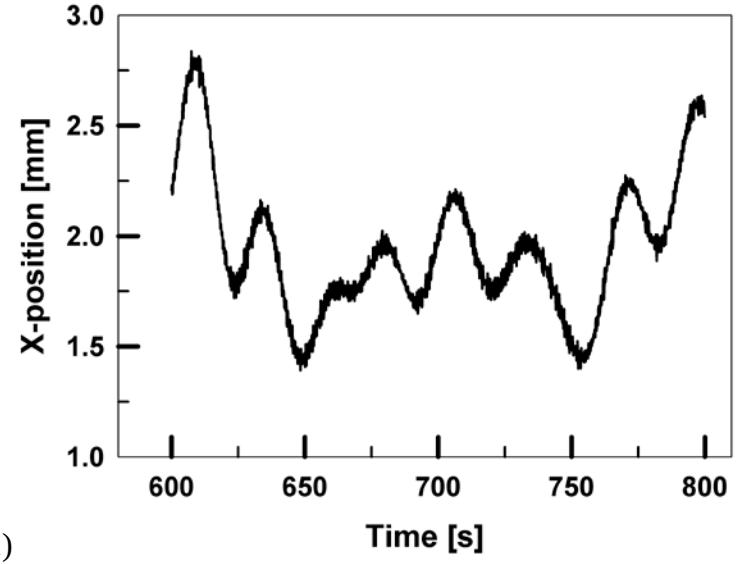
X-position [mm]
3.0
2.5
2.0
1.5
1.0
600
650
700
750
800
Time [s]

(b1)

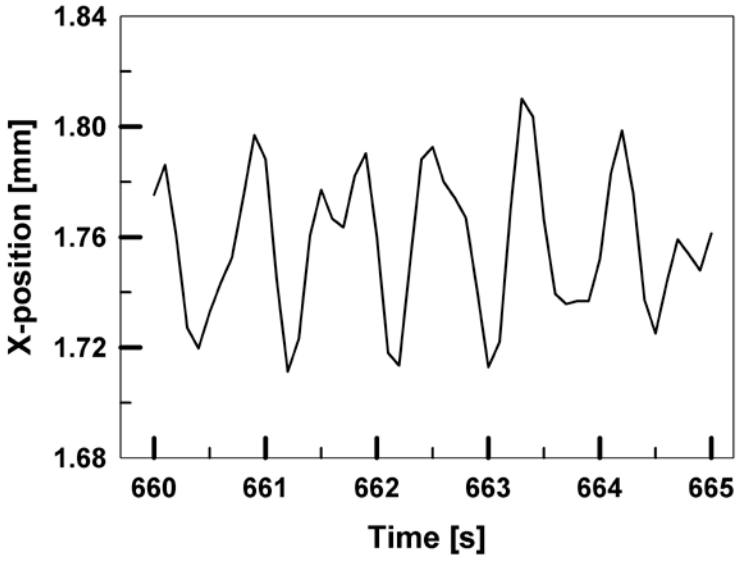
1.84
1.80
1.76
1.72
1.68
X-position [mm]
660
661
662
663
664
665
Time [s]

(b2)

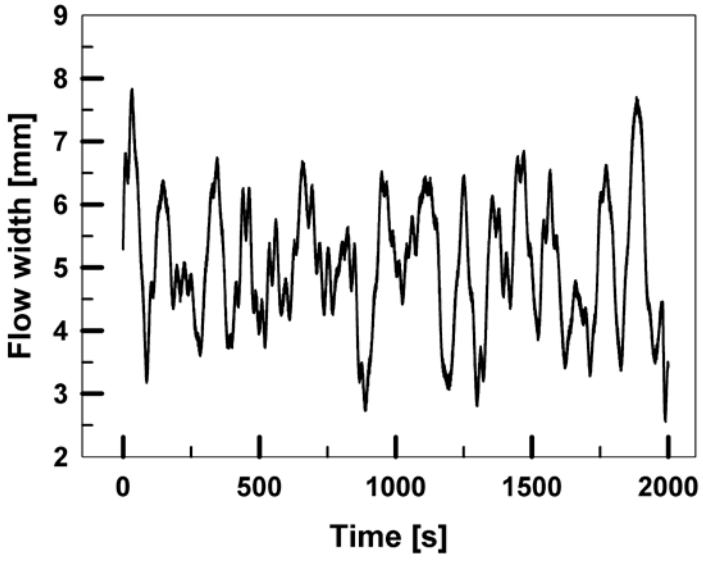
9
8
7
6
5
4
3
2
Flow width [mm]
0
500
1000
1500
2000
Time [s]

(c1)

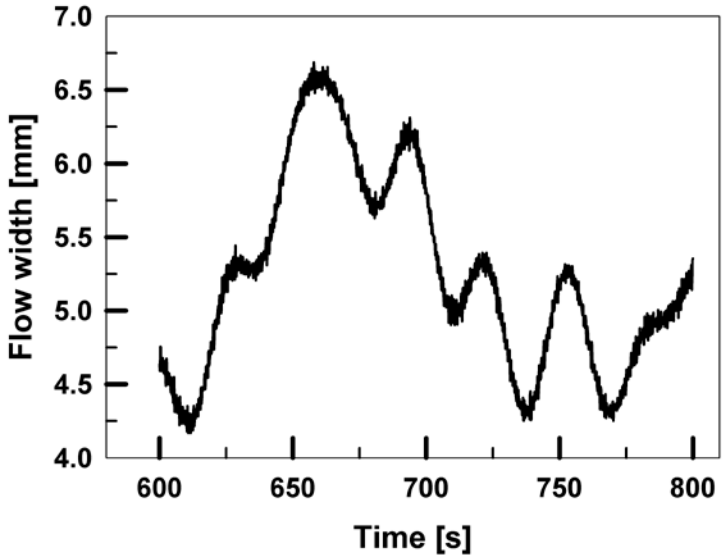
Flow width [mm]
7.0
6.5
6.0
5.5
5.0
4.5
4.0
600
650
700
750
800
Time [s]

(c2)

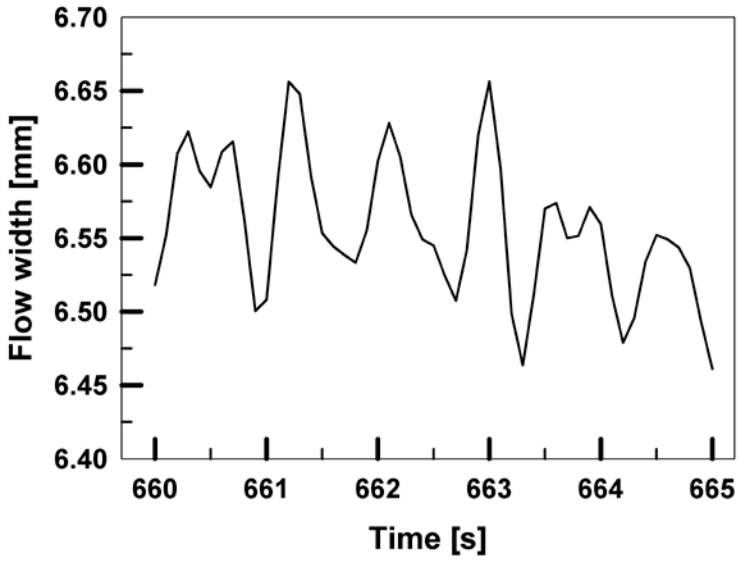
Flow width [mm]
6.70
6.65
6.60
6.55
6.50
6.45
6.40
660
661
662
663
664
665
Time [s]

(c3)

Figure 4.15. Flow boundary fluctuation of pH 9.5 40vol% alumina suspension between flow regime and no-flow regime and width of flow regime as a function of time at shear rate $0.1s^{-1}$, (a) fluctuation of left and right flow boundary, (b1) fluctuation of left flow boundary in time scale of 200s, (b2) fluctuation of left flow boundary in time scale of 5s, (c1) fluctuation of flow width in time scale of 2000s, (c2) fluctuation of flow width in time scale of 200s, (c3) fluctuation of flow width in time scale of 5s

Figure 4.15(b1) and (b2) are the enlarged graphs of change in the left side of the flow boundary in figure 4.15(a) at 200 second and 5 second time scale, respectively. Figure 4.15(c1) is a graph of the change in the distance between the no-flow region at the left side and the no-flow region at the right side over time, with the values of right-side boundary subtracted by left-side boundary. Figure 4.15(c2) and 8(c3), like the figure 4.15(b1) and (b2), show the data from figure 4.15(c1) in 200 second and 5 second time scale, respectively.

As can be seen in figure 4.15(a), the flow boundary exhibited a large fluctuation with a period of few hundred seconds. The oscillation width was about 45% of the channel's width (10 mm). The data for the left and right boundary exhibited 80~120 seconds of time gap with reference to the maximum points. The width of the flow region between the no-flow regions demonstrated fluctuation in accordance with this time gap (figure 4.15(c1)). As can be seen in figure 4.15(c1), the width of the flow region also exhibited fluctuation with time scale of a few hundred seconds. The time period of this fluctuation was less than that of the fluctuation of one boundary. The oscillation width of the flow regime was about 70% (7mm) of the channel width with the minimum of 1 mm to the maximum of 8 mm. In addition to the large fluctuations with periods of a few hundred seconds, smaller fluctuations with periods of a few dozens of seconds. As depicted in figure 4.15(b1), the smaller fluctuations had oscillation widths of about 12.5% (1.25mm) of the channel width and periods of 20~50 seconds. Furthermore, fluctuations of even smaller oscillation width and periods were observed

(figure 4.15(b2)). The oscillation period in figure 4.15(b2) is less than 1 second with oscillation widths of about 0.8% (0.08mm) of the channel width. This showed minute oscillations of the continuous flow boundaries. The effects of medium fluctuations of one side of the flow boundary with periods of few dozen seconds and minute fluctuations with periods less than a second could be observed in case of fluctuation of channel width (figure 4.15(c2) and (c3)).

In the regions where the shear stress increases monotonically with the shear rate, the flow profile shown in figure 4.14(b) was maintained stably. The fluctuations with long or medium periods depicted in figure 4.15 were not observed. The oscillations with minute periods and widths shown in figure 4.15(c3) were observed in this region, however.

In order to more accurately analyze the oscillation width and period of the flow boundary and the flow region in figure 4.15, Fourier transform analysis was performed. The results are depicted in figure 4.16.

Figure 4.16 represents the Fourier transform analysis results of the oscillation width of the flow region in figure 4.15(c1). Peaks representing the oscillation periods are observed around the frequency of 2Hz. These peaks could be divided into two groups of low frequency characteristic peak and high frequency characteristic peak. The low frequency region (~0.05Hz) is represented in figure 4.16(b). The high frequency region (1.0Hz~2.0Hz) is represented in figure 4.16(c).

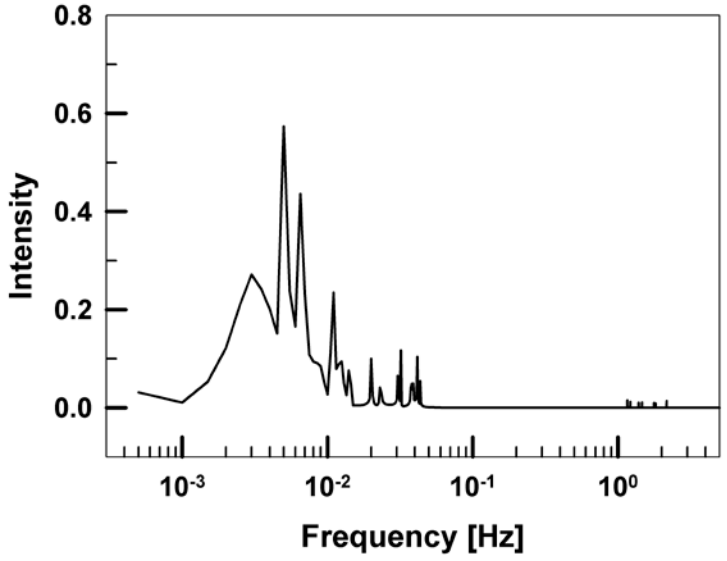
0.8
0.6
0.4
0.2
0.0
Intensity
10-3
10-2
10-1
100
Frequency [Hz]

(a)

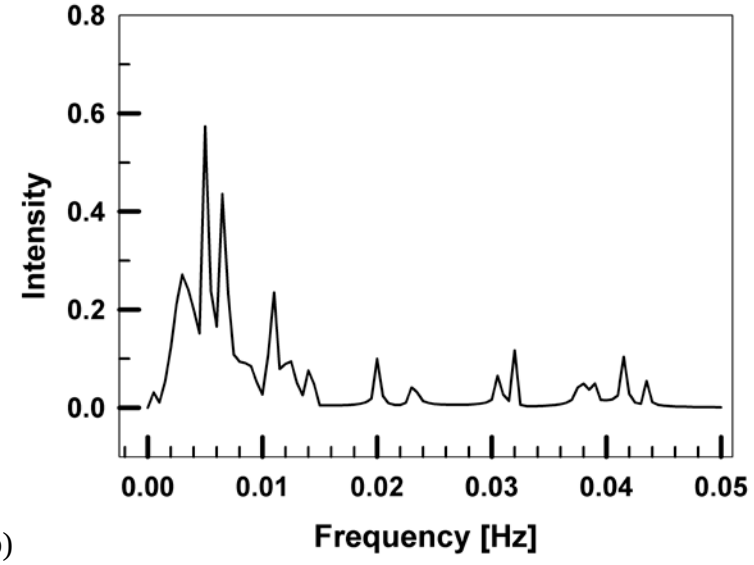
0.8
0.6
0.4
0.2
0.0
Intensity
0.00
0.01
0.02
0.03
0.04
0.05
Frequency [Hz]

(b)

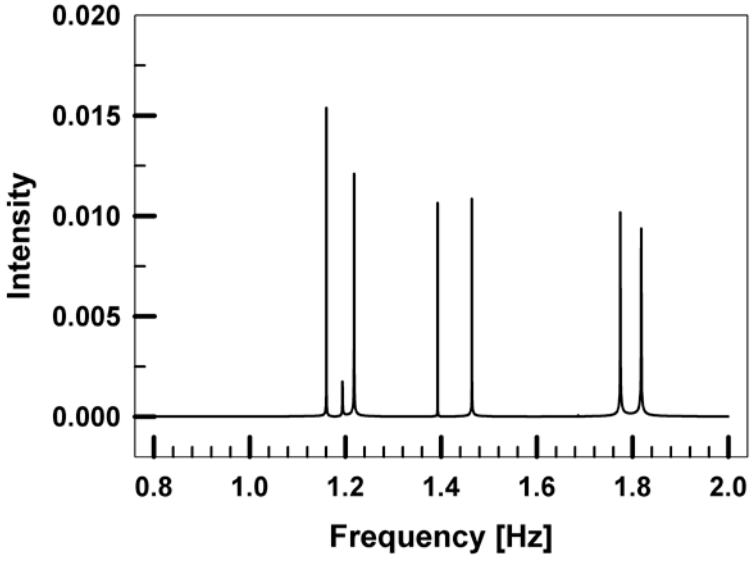

(c)

Figure 4.16. Fourier transform result of fluctuation of flow regime width in figure 4.15(c1), (a) FT result in frequency range of ~5Hz, (b) FT result in low frequency range of ~0.05Hz, (c) FT result in frequency range between 0.8Hz and 2.0Hz

In the low frequency region of figure 4.16(b), 5~6 characteristic peaks were observed. These peaks can again be divided into two groups by their frequencies (0~0.1Hz for one group and 0.01Hz to 0.05Hz for another group). For the lowest frequency characteristic peaks, the highest intensity peak, which is the fluctuation's main characteristic peak, had the frequency of 0.05Hz. This corresponds to the time period of 200 seconds, which represents the large oscillations with long periods in figure 4.15(c1). The secondary peak and the third characteristic peak in this group are at 0.065Hz (154 second) and 0.01Hz (100 second), which also have hundred second time periods. The characteristic peaks in the 0.01Hz~0.05Hz frequency group are at 0.02Hz, 0.032Hz, 0.043Hz, which represent 50second, 32 second, and 24 second. These correspond to the medium oscillations with a few dozen second periods, shown in figure 4.15(c2). The small amplitude and period oscillations in figure 4.15(c3) are represented well by the 1Hz~2Hz characteristic peaks in figure 4.16(c). The characteristic peaks in figure 4.16(c) are at 1.2Hz (0.83 second), 1.4Hz (0.71 second), and 1.8Hz (0.56 second) with very small intensity. These represent well the oscillations with minute width and period less than 1 second, shown in figure 4.15(c3).

4.4.2 Pressure fluctuation and its relation to flow instability

In the stress decay region with non-homogenous and time periodic flow profile change, the pH 9.5 40vol% alumina suspension exhibited large, time periodic pressure fluctuation instead of steady pressure behavior. This pressure fluctuation behavior is shown in figure 4.17.

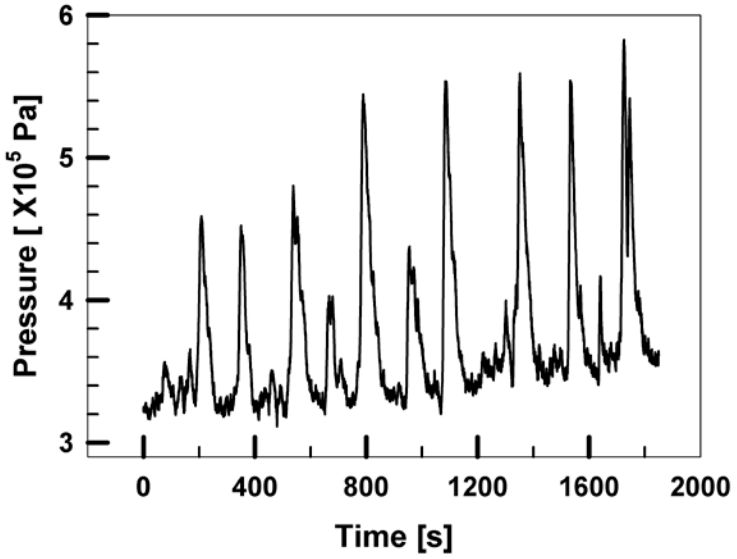
Pressure [X10^5 Pa]
6
5
4
3
0
400
800
1200
1600
2000
Time [s]

(a)

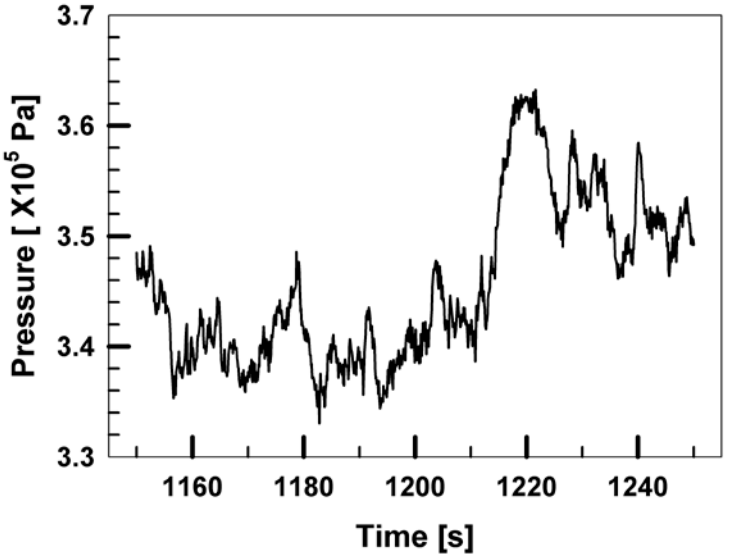
Pressure [X10^5 Pa]
3.7
3.6
3.5
3.4
3.3
1160
1180
1200
1220
1240
Time [s]

(b)

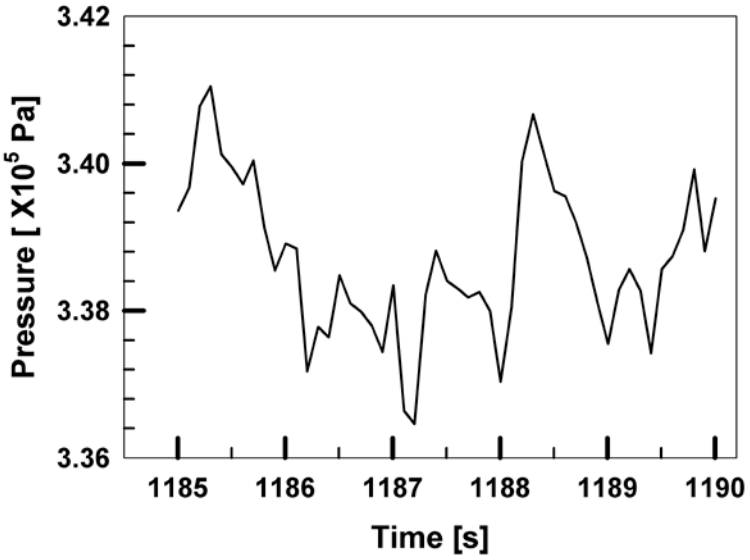

(c)

Figure 4.17. Pressure fluctuation of pH 9.5 40vol% alumina suspension at shear rate 0.1s-1 measured at the same time of flow visualization, (a) pressure fluctuation in time scale of 2000s, (b) pressure fluctuation in time scale of 100s, (c) pressure fluctuation in time scale of 5s

The graph in figure 4.17 represents the data for pressure oscillation of pH 9.5 40vol% alumina suspension at shear rate of $0.1s^{-1}$. Figure 4.17(a) is the pressure fluctuation in time scale of 2000 second. Figure 4.17(b) and (c) represent 100 second time scale and 5 second time scale, respectively. As can be seen in figure 4.17(a), pressure fluctuation with large amplitude (approximately 80%) and long time period was observed even at a constant shear rate. In addition, pressure fluctuations with medium amplitude (approximately 10%) and a few dozen second time period and fluctuations with very small period and amplitude (approximately 1.2%) were observed.

The pressure fluctuations exhibited the same trend that the flow region fluctuation in figure 4.15 showed. The flow boundary and flow region width fluctuation in figure 4.15 could also be divided into three groups (fluctuations with a few hundred second period and 70% amplitude, fluctuations with a few dozen second period and 12~25% amplitude, and fluctuations with less than 1 second period and less than 1% amplitude), similar to the trend of the pressure fluctuation behavior. In the region where the stress increase monotonically with the shear rate, the 40vol% alumina suspension displayed a stable flow profile (figure 4.13(b)). The pressure in this region also fluctuated with very small amplitude (less than 1%) and immeasurable time period. Large amplitude pressure fluctuation could not be observed in figure 4.17.

This pressure fluctuation behavior has been reported in a previous study of shear banding worm micelle solution (Ganapathy and Sood 2008). In this study, the wormlike micelle solution exhibited stress plateau at certain shear

rates. The shear-banding phenomenon in this region has been optically analyzed and reported. The shear stress in this shear-banding region exhibited fluctuation behavior with certain periods at certain shear rates. This shear stress time periodic fluctuation behavior disappeared outside the stress plateau region, changing into chaotic fluctuation with uncertain time period. Similar to this study, the 40vol% coagulated alumina suspension exhibited shear-banding behavior in the region where the shear stress decreases with the increase in shear rate. The pressure also fluctuated with certain period. However, in our research, the pressure fluctuations had multiple periods (in three groups) at one shear rate, unlike the worm micelle solution's single period fluctuation at one shear rate. The flow profile also did not maintain a constant shear-banded profile, but changed over time.

As was done with the Fourier transform analysis for time period in figure 4.18, the pressure fluctuation in figure 4.17 was also analyzed using Fourier transform, represented in figure 4.18. Figure 4.18 represents the Fourier transform analysis on the pressure fluctuation data in figure 4.17(a). The characteristic peaks that represent pressure fluctuation periods are observed around the frequency of 2Hz. These characteristic peaks, similar to the flow region width fluctuation data, can be divided by their frequencies into two groups of low frequency region characteristic peaks and high frequency region characteristic peaks. The low frequency region (about 0.05Hz) is shown in figure 4.18(b). The high frequency region (1.0Hz~2.0Hz) is shown in figure 4.18(c).

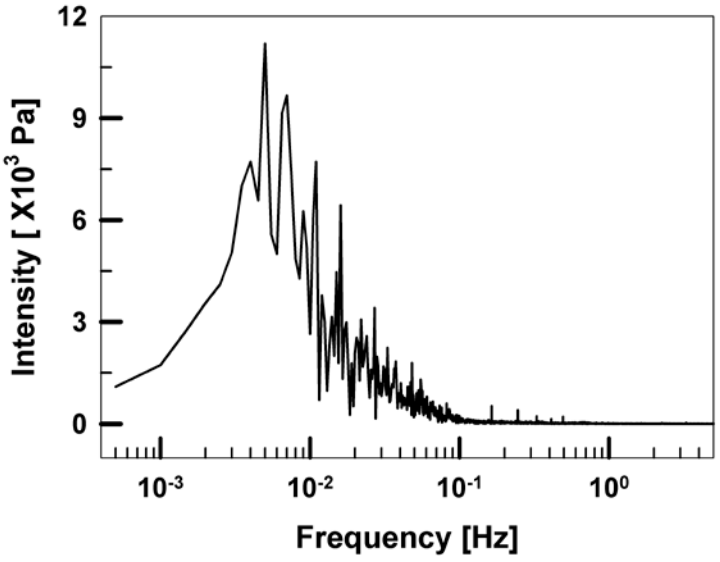
12
9
6
3
0
Intensity [X10^3 Pa]
10^{-3}
10^{-2}
10^{-1}
10^0
Frequency [Hz]

(a)

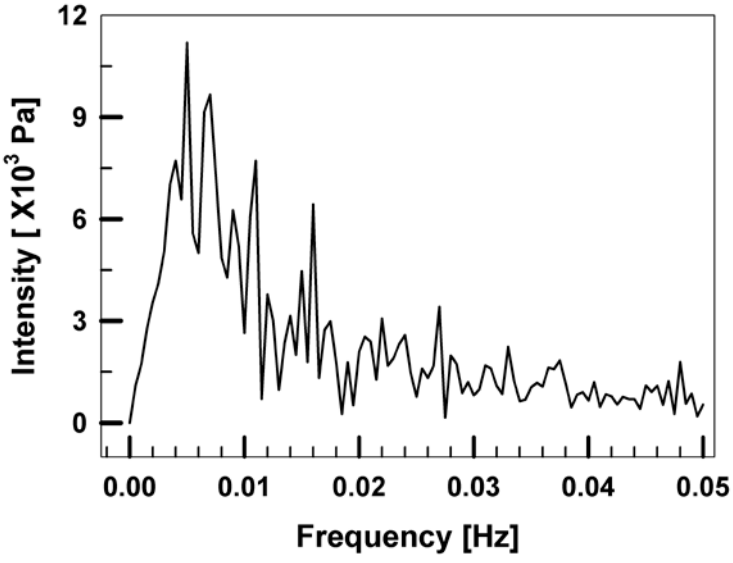
12
9
6
3
0
Intensity [X10^3 Pa]
0.00
0.01
0.02
0.03
0.04
0.05
Frequency [Hz]

(b)

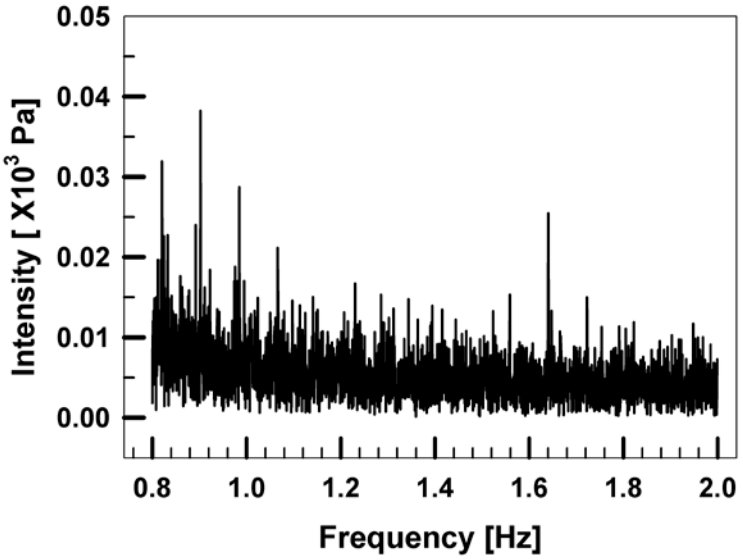

(c)

Figure 4.18. Fourier transform result of pressure fluctuation in figure 4.17(a), (a) FT result in frequency range of ~5Hz, (b) FT result in low frequency range of ~0.05Hz, (c) FT result in frequency range between 0.8Hz and 2.0Hz

The pressure fluctuation Fourier transform result exhibited more characteristic peaks than the flow region width Fourier transform result. However, same with the width Fourier transform result, there were 5 to 6 characteristic peaks in the low frequency region. These peaks could be divided into two groups depending on the time periods (the region up to 0.01 Hz and the region from 0.01Hz to 0.05Hz). The main peak with the strongest intensity had the frequency of 0.05Hz, same with the result from figure 4.16. The second and third characteristic peaks also had frequencies in the range of 0.007Hz to 0.01Hz, same or similar to the flow width fluctuation results. The characteristic peaks in the 0.01Hz~0.05Hz frequency were located at 0.016Hz, 0.027Hz, and 0.05Hz, similar to the flow width fluctuation results with slight longer time periods. The very small intensity characteristic peaks in figure 4.18(c) were located at 0.9Hz, 1.37Hz, and 1.64 Hz, which is similar to the flow width fluctuation peaks like in the cases of strong intensity peaks. These peaks show the very small amplitude pressure fluctuations with less than 1 second time periods depicted in figure 4.17(c).

As can be observed from the results in figure 4.14 ~ figure 4.18, the pressure fluctuation behavior and the flow profile change (the fluctuation behavior) exhibited very similar results. Both results showed three types of fluctuations (large amplitude fluctuations with long time periods, medium time period and medium amplitude fluctuations, and very small amplitude and short time period fluctuations). Each type of fluctuations had similar time periods for both the pressure behavior and the flow profile behavior.

Therefore, it can be concluded that the flow profile change inside the slit channel is closely related to the pressure fluctuation.

The pressure drop measured at a certain flow velocity or at a certain shear rate is a function of the width of the channel that the fluid flows through. As the width decreases, the pressure increases. Unlike the Newtonian fluids or well-dispersed suspensions, the 40vol% coagulated alumina suspension formed wide no-flow regions inside the channel. This no-flow region did not maintain constant width or location, but changed with time. The transient change exhibited time periodic trends. Therefore, it can be stated that the flow region changes due to the periodic change of the no-flow region. It can also be stated that this change is the reason for the pressure fluctuation.

In this study, it was observed that coagulated alumina suspension with high solid concentration exhibited a very complex flow profile change in the slit channel during the solid-liquid transition process, unlike the same suspension with lower concentration. This flow profile change had time periodic behavior with multiple periods. In addition, the pressure fluctuation from the pressure measurements exhibited nearly the same period and amplitude with the flow profile fluctuation. From this, it was concluded that the complex flow profile inside the channel is the cause of the pressure fluctuation, the pressure and the flow profile having very close relationship.

Chapter 5. Conclusion

The slit channel flows of alumina suspensions with two different dispersion states, coagulated system and well-dispersed system, were analyzed, and the complex flow behavior and the flow development in solid-liquid transition process were quantitatively described in terms of flow profile and pressure fluctuation with modified capillary rheometer including in-situ flow visualization system.

For the coagulated system, the flow of pH 9.5 25vol% alumina suspension exhibited shear banded flow profile with no-flow or sluggish flow rate closed to the channel wall and plug flow at channel center in certain shear rate region in which the shear stress decreased. At this region, the pressure exhibited time periodic fluctuation. In the region of monotonically increase of shear stress, this fluid represented plug-like flow with small pressure fluctuation having no certain time periodicity. By observing the transient flow over time at high shear rate, it was shown that the flow profile sequence was developed in similar way with the change of flow profile of the steady state flow at lower shear rate. From this, it was analyzed that the flow profile change in the stress-decay region was due to the discrete solid-liquid transition process and that the flow profile in this transition process exhibited shear banded flow. As the solid concentration increased for the coagulated system, the flow profile in the solid-liquid transition region (stress-decay region) exhibited more complex flow behavior. The pH 9.5 40vol% alumina suspension exhibited a complex flow behavior of very large no-flow region along with an asymmetric flow. Such flow profile exhibited three different fluctuations (fluctuation over long period of

time with large amplitude, medium amplitude and medium period fluctuation, and a very short period, small amplitude fluctuation). FT analysis was applied to quantitatively analyze these fluctuations. The pH 9.5 40vol% alumina suspension also exhibited time periodic pressure fluctuation. The FT analysis revealed that this pressure fluctuation had the same time period with the flow profile fluctuation. Therefore, it was determined that the flow profile change in the slit channel had close relationship with the pressure change and that the pressure fluctuation is caused by the complex flow behavior inside the channel.

For the well-dispersed system, the 25 vol% well-dispersed alumina suspension which showed monotonic increase of shear stress, only the plug-like flow was observed with small pressure fluctuation without any characteristic time periodicity. But, the concentrated suspensions with higher solid concentration (55vol% and 40vol%) showed different flow behavior from that of Newtonian fluid or the suspension with less concentration (25vol%). At low shear rate, these highly concentrated alumina suspensions exhibited a unique transient behavior in which there was no flow at first and fluid began to flow from the center regime. The flow regime expanded to the whole domain in the channel and finally reached to a flow profile having two inflection points which was banded by the region with sluggish flow rate near the channel wall, the region with rapid increase to maximum, and the region of plug flow. This unique and complex flow profile was strongly correlated with stress plateau as same as the case of coagulated suspensions; these shear banded flow profile was observed only in stress plateau.

This study has visualized the flow behavior of highly concentrated alumina suspension in a slit channel during the solid-liquid transition and quantitatively analyzed the visualization results. From this, it was determined that the highly concentrated alumina suspension exhibited shear banded flow profile during the solid-liquid transition process. In addition, by analyzing the flow profile behavior with the pressure fluctuation, it was decided that the complex flow behavior inside the channel could be analyzed from the pressure fluctuation. The visualization and the quantitative analysis results in this study for the diverse fluids including highly concentrated particulate fluids can be expected to contribute greatly to the process analysis and process designs in a slit channel or for the capillary flows, which are similar to the actual industrial processes.

Reference

Azzouzi H, Decruppe JP, Lerouge S, Greffier O (2005) Temporal oscillations of the shear stress and scattered light in a shear banding-shear thickening micellar solution. Eur. Phys. J. E 17: 507-514

Barnes HA (1989) Shear-Thickening ("Dilatancy") in Suspensions of Nonaggregating Solid Particles Dispersed in Newtonian Liquids. Journal of Rheology 33: 329-336

Baudez JC, Rodts S, Chateau X, Coussot P (2004) New technique for reconstructing instantaneous velocity profiles from viscometric tests:Application to pasty materials. Journal of Rheology 48: 69-83

Berret JF, Roux DC, Porte G, Lindner P (1994) Shear-Induced Isotropic-to-Nematic Phase Transition in Equilibrium Polymers. Europhysics Letters 25: 521-526

Bertola V, Bertrand F, Tabuteau H, Bonn D, Coussot P (2003) Wall slip and yielding in pasty materials. Journal of Rheology 47: 1211-1226

Besseling R, Isa L, Ballesta P, Petekidis G, Cates ME, Poon WCK (2010) Shear banding and flow-concentration coupling in colloidal glasses. Physical Review Letters 105: 268301

Besseling R, Isa L, Weeks ER, Poon WCK (2009) Quantitative imaging of colloidal flows. Advances in Colloid and Interface Science 146: 1-17

Cappelaere E, Berret JF, Decruppe JP, Cressely R, Lindner P (1997) Rheology, birefringence, and small-angle neutron scattering in a charged micellar system: Evidence of a shear-induced phase transition. Physical Review E 56: 1869-1878

Channell G. M., Miller K. T., and Zukoski C. F. (2000) “Effects of Microstructure on the Compressive yield stress”, AlChE journal 46(1): 72-78

Cohen I, Davidovitch B, Schofield AB, Brenner MP, Weitz DA (2006) Slip, yield, and bands in colloidal crystals under oscillatory shear, Physical Review Letters 97: 215502-215504

Cohen I, Mason TG, Weitz DA (2004) Shear-induced configurations of confined colloidal suspensions. Physical Review Letters 93: 046001-046004

Coussot P (2005) Rheometry of pastes, suspensions, and granular materials : applications in industry and environment. John Wiley & Son, New Jersey

Coussot P, Raynaud JS, Bertrand F, Moucheront P, Guilbaud JP, Huynh HT, Jarny S, Lesueur D (2002) Coexistence of Liquid and Solid Phases

in Flowing Soft-Glassy Materials. Physical Review Letters 88: 218301

Coussot P, Tocquer L, Lanos C, Ovarlez G (2008) Macroscopic vs. local rheology of yield stress fluids. Journal of Non-Newtonian Fluid Mechanics 158: 85-90

Derks D, Wisman H, van Balaaderen A, Imhof A (2004) Confocal microscopy of colloidal dispersions in shear flow using a counter-rotating cone-plate shear cell. Journal of Physics-Condensed Matter 16: S3917-S3927

Dhont JG and Briels W (2008) Gradient and vorticity banding. Rheol Acta 47: 257-281.

Dusschoten D and Wilhelm M (2001) Increased torque transducer sensitivity via oversampling. Rheol Acta 40: 395-399

Fernández VVA et al. (2009) Rheology of the Pluronic P103/water system in a semidilute regime: Evidence of nonequilibrium critical behavior. Journal of Colloid and Interface Science 336: 842-849

Fielding SM (2005) Linear instability of planar shear banded flow. Phys. Rev. Lett., 95: 134501-134504

Fielding SM (2007) Complex dynamics of shear banded flows. Soft Matter 3: 1262-1279

Fielding SM , Olmsted PD (2004) Spatiotemporal oscillations and rheochaos in a simple model of shear banding. Phys. Rev. Lett., 92: 845021-8845024

Fielding SM , Olmsted PD (2006) Nonlinear dynamics of an interface between shear bands. Phys. Rev. Lett., 96: 104502-104504

Fielding SM and Wilson HJ (2010) Shear banding and interfacial instability in planar Poiseuille flow. Journal of Non-Newtonian Fluid Mechanics 165: 196-202

Fisher P, Wheelar EK, Fuller GG (2002) Shear-banding structure orientated in the vorticity direction observed for equimolar micellar solution. Rheol. Acta 41: 35-44

Ganapathy R and Sood AK (2008) Nonlinear flow of wormlike micellar gels; Regular and chaotic time-dependence of stress, normal force and nematic ordering. Journal of Non-Newtonian Fluid Mechanics 149: 78-86

Garcı´a-Sandoval JP, Manero O, Bautista F, Puig JE (2012) Inhomogeneous flows and shear banding formation in micellar solutions: Predictions of the BMP model. Journal of Non-Newtonian Fluid Mechanics 179: 43-54

Hernández-Acosta S, González-Alvarez A, Manero O, Méndez Sánchez AF, Pérez-González J, de Vargas L (1999) Capillary rheometry of

micellar aqueous solutions. Journal of Non-Newtonian Fluid Mechanics 85: 229-247

Hoffman R (1998) Explanations for the cause of shear thickening in concentrated colloidal suspensions. Journal of Rheology 42: 111-124

Holmes WM, Callaghan PT, Vlassopoulos D, Roovers J (2004) Shear banding phenomena in ultrasoft glasses. J. Rheol. 48: 1085-1102

Holmqvist P, Daniel C, Hamley IW, Mingvanish W, Booth C (2002) Inhomogeneous flow in a micellar solution of a diblock copolymer: creep rheometry experiments. Colloids and Surfaces A: Physicochemical and Engineering Aspects 196: 39-50

Hunter RJ (1993) Introduction to modern colloid science. New York, Oxford press

Isa L, Besseling R, Poon WCK (2007) Shear zones and wall slip in the capillary flow of concentrated colloidal suspensions. Physical Review Letters 98: 198305

Isa L, Besseling R, Poon WCK (2007) Shear zones and wall slip in the capillary flow of concentrated colloidal suspensions. Physical Review Letters 98: 198305

Johnson SB, Franks GV, Scales PJ, Boger DV, Healy TW (2000) Surface chemistry–rheology relationships in concentrated mineral suspensions. International Journal of Mineral Processing 58: 267-304

Johnson SB, Russell AS, Scales PJ (1998) Volume fraction effects in shear rheology and electroacoustic studies of concentrated alumina and kaolin suspensions. Colloids and Surfaces A: Physicochemical and Engineering Aspects 141: 119-130

Kabla A, Debregeas G (2003) Local stress relaxation and shear banding in a dry foam under shear. Phys. Rev. Lett. 90: 2583031-2583034

Kim S, Sung JH, Ahn KH, Lee SJ (2009) Rheological perspectives on industrial coating process. Korea-Australia Rheology Journal 21: 83-89

Lee YS, Wetzel ED, Wagner NJ (2003) The ballistic impact characteristics of Kevlar® woven fabrics impregnated with a colloidal shear thickening fluid. Journal of Materials Science 38: 2825-2833

Lerouge S, Aregentina M, Decruppe JP (2006) Interface instability in shear banding flow. Phys. Rev. Lett., 96: 0883011-0883014

Lootens D, van Damme H, Hémar Y, Hébraud P (2005) Dilatant Flow of Concentrated Suspensions of Rough Particles. Physical Review Letters 95: 268302

Mair RW, Callaghan PT (1997) Shear flow of wormlike micelles in pipe and cylindrical Couette geometries as studied by nuclear magnetic resonance microscopy. Journal of Rheology 41: 901-924

Manneville S (2008) Recent experimental probes of shear banding. Rheol Acta 47: 301-318.

Manneville S, Salmon JB, Becu L, Colin A, Molino F (2004) Inhomogeneous flow in sheared complex fluids, Rheol. Acta 47: 301-318

Mansard V and Colin A (2012) Local and non local rheology of concentrated particles. Soft Matter 8: 40254043

Maranzano BJ and Wagner NJ (2001a) The effects of interparticle interactions and particle size on reversible shear thickening: Hard-sphere colloidal dispersions. Journal of Rheology 45: 1205-1222

Maranzano BJ and Wagner NJ (2001b) The effects of particle size on reversible shear thickening of concentrated colloidal dispersions. Journal of Chemical Physics 114: 10514-10527

Marín-Santibáñez BM, Pérez-González J, de Vargas L, Decruppe JP, Huelsz G (2009) Visualization of shear banding and entry Poiseuille flow oscillations in a micellar aqueous solution. Journal of Non-Newtonian Fluid Mechanics 157: 117-125

Masselon C, Salmon JB, Colin A (2008) Nonlocal effects in flows of wormlike micellar solutions. Physical Review Letter 100: 038301

Mewis J and Wagner NJ (2012) Colloidal suspension rheology, Cambridge University Press, New York

Miller E and Rothstein JP (2007) Transient evolution of shear-banding wormlike micellar solutions. Journal of Non-Newtonian Fluid Mechanics 143: 22-37

Olmsted P (2008) Perspectives on shear banding in complex fluids. Rheol Acta 47: 283-300.

Olmsted PD, Goldbart P (1990) Theory of the nonequilibrium phase-transition for newmatic liquid-crystal under shear flow. Phys. Rev. A 41: 4578-4581

Ovarlez G, Rodts S, Chateau X, Coussot P (2009) Phenomenology and physical origin of shear localization and shear banding in complex fluids. Rheol Acta 48: 831-844.

Partal P, Kowalski AJ, Machin D, Kiratzis N, Berni MG, Lawrence CJ (2001) Rheology and Microstructural Transitions in the Lamellar Phase of a Cationic Surfactant. Langmuir 17: 1331-1337.

Rehage H, Hoffmann H (1991) Viscoelastic surfactant solutions: model systems for rheological research. Molecular Physics 74: 933-973.

Rodts S, Baudez JC, Coussot P (2005) From “discrete” to “continuum” flow in foams. Europhys Lett 69: 636-642

Salmon J-B, Manneville S, Colin A (2003) Shear banding in a lyotropic lamellar phase. I. Time-averaged velocity profiles. Physical Review E 68: 051503

Schmitt V, Lequeux F, Pousse A, Roux D (1994) Flow Behavior and Shear Induced Transition near an Isotropic/Nematic Transition in Equilibrium Polymers. Langmuir 10: 955-961.

Schmitt V, Lequeux F, Pousse A, Roux D (1994) Flow Behavior and Shear Induced Transition near an Isotropic/Nematic Transition in Equilibrium Polymers. Langmuir 10: 955-961.

Shaw DJ (1970) Introduction to colloid and surface science. London, Butterworth & Co. Ltd

Shereda, LT, Larson RG, Solomon MJ (2010) Shear banding in crystallizing colloidal suspensions, Korea-Australia Rheol. J. 22: 309-316

Tapadia P, Ravindranath S, Wang SQ (2006) Banding in entangled polymer fluids under oscillatory shearing. Physical Review Letters 96: 196001-196004

Tapadia P, Wang SQ (2004) Nonlinear flow behavior of entangled polymer solutions: Yieldlike entanglement-disentanglement transition.

Macromolecules 37: 9083-90995

Tapadia P, Wang SQ (2006) Direct visualization of continuous simple shear in non-Newtonian polymeric fluids. Phys. Rev. Lett. 96: 016001-016004

Wang SQ (2007) A coherent description of nonlinear flow behavior of entangled polymers as related to processing and numerical simulations. Macromolecular Materials and Engineering 292: 15-22

Wang SQ (2007) A coherent description of nonlinear flow behavior of entangled polymers as related to processing and numerical simulations. Macromolecular Materials and Engineering 292: 15-22

Wilson HJ, Fielding SM (2006) Linear instability of planar shear banded flow of both diffusive and non-diffusive Johnson-Segalman fluids. JNNFM 138: 181-196

Wu YL, Derks D, van Blaaderen A, Imhof A (2006) Melting and crystallization of colloidal hard-sphere suspensions under shear. Proc. Natl. Acad. Sci. USA 106: 10564-10569

Yamamoto T, Hashimoto T, Yamashita A (2008) Flow analysis for wormlike micellar solutions in an axisymmetric capillary channel. Rheol. Acta 47: 963-974

Yesilata B, Clasen C, McKinley GH (2006) Nonlinear shear and extensional

flow dynamics of wormlike surfactant solutions. JNNMF 133: 73-90

국문초록

압력 구배 흐름에서의 고농도 알루미나 현탁액의 복잡거동

한우주

서울대학교 대학원

화학생물공학부

본 논문에서 고농도 입자계 현탁액의 압력 구배 흐름에서의 유동을 이해하기 위한 새로운 방법을 제시하였다. 두 가지 분산상태, 입자끼리 응집이 강한 상태와 안정적으로 분산되어 있는 상태, 를 가지는 고농도 알루미나 현탁액의 유동을 모세관 점도계의 개량을 통해 사각채널에서 가시화 하였다. 본 논문에서 현탁액의 고체-액체 전이 거동을 포함한 여러 복잡 거동을 유동장 형태 분석과 압력 진동 분석을 통해 정량적으로 설명하고자 하였다.

고농도 알루미나 현탁액은 여러 복잡 거동, 독특한 고체-액체 전이와 전단 구부러짐 현상(Shear banding), 을 보였다. 초기 정지 거동과 이후 시간에 따른 연속적인 유동장 변화를 포함하는 고체-액체 전이 거동을 관찰할 수 있었으며, 특히 낮은 유동 속도에서는 채널 벽 근처에서의 현저히 정체된 유동속도와 두 개의 변곡점을 가지는 독특한 형태의 전단

구부러짐 형태의 유동장을 관찰할 수 있었다. 또한 본 연구에서 이러한 사각 채널에서의 전단 구부러짐 현상이 전단 응력 거동과 매우 밀접한 상관 관계를 가지는 것을 확인하였다.

응집 상태의 현탁액의 경우, 전단 응력은 전단 속도에 따라 감소하였다가 다시 증가하는 N 자 형태의 곡선을 보였다. 이러한 전단응력 거동에 따라 유동장은 두 가지 형태로 구분할 수 있었다. 즉, 전단 속도에 따라 전단 응력이 감소하는 영역에서의 유동장은 채널 벽 근처에서 유동이 없거나 현저히 정체된 전단 구부러짐 형태의 유동을 보였으며, 전단 응력이 단순 증가하는 영역에서는 뉴튼 유체와 유사한 플러그 흐름(Plug-like flow)을 보였다. 또한 이 응집 상태의 알루미나 현탁액은 높은 유동 속도에서의 시간에 따른 유동장 변화와 고체-액체 전이 영역 (전단 응력이 감소하는 영역) 에서의 낮은 유동 속도에서의 정상 상태 흐름 (steady state flow) 변화와 매우 유사한 현상을 보였다. 덧붙여 위의 전이 과정에서의 전단 구부러짐 형태의 유동에서의 압력 역시 일정한 값이 아닌 특정 시간 주기를 가지는 압력 진동 거동을 보였다. 입자 농도가 증가할 수록 이 응집 상태의 현탁액은 고체-액체 전이 영역에서 매우 넓은 흐름이 없는 영역과 비대칭의 유동 형태로 나타나는 좀 더 복잡한 거동을 보였다. 압력 진동 거동과 유동장 변화를 퓨리에 변환 (Fourier transform) 변환 방법을 통해 분석한 결과, 압력 진동과 유동장 변화는 매우 유사한 특정 시간 주기를 가지며 결과적으로 둘이 매우 밀접한 상관관계를 가진다는 것을 확인하였다.

응집 상태의 현탁액과는 달리, 낮은 농도의 안정된 분산 상태의 현탁액은 단순 증가하는 전단 응력 거동과 플러그 흐름 만을 보였다. 그러나 이

현탁액도 입자 농도가 증가할 수록 응집 상태의 현탁액과 마찬가지로 독특한 고체-액체 전이 현상과 전단 구부러짐 형태의 유동장을 보였다.

본 연구에서 고농도 알루미나 현탁액의 사각 채널에서의 전단 구부러짐 현상을 가시화 하였으며 이를 정량적으로 분석하였다. 이러한 연구 결과는 실제 산업 공정의 대표적인 유동 형태인 압력 구배 흐름에서 입자계 유체의 유동을 이해하고 제어하는데 효과적인 방법이 될 것으로 예상할 수 있다.

주제어: 복잡 유동, 전단 구부러짐 현상, 압력 구배 흐름, 고농도 현탁액, 고체-액체 전이, 압력 진동

학 번: 2006-21394